Questionnaire surveys on damages at high-rise buildings and synthesized near-fault long-period strong ground motions of the 2018 Hualien, Taiwan, earthquake

Xin Wang [f,*], Masayuki Nagano [a], Hongjun Si [b], Wen-Yen Chang [c], Chun-Hsiang Kuo [d], Che-Min Lin [e]

[a] Tokyo University of Science, Chiba, Japan
[b] Seismological Research Institute Inc., Tokyo, Japan
[c] National Dong Hwa University, Hualien, Taiwan
[d] National Central University, Taoyuan, Taiwan
[e] National Center for Research on Earthquake Engineering, Taipei, Taiwan
[f] Ashikaga University, Tochigi, Japan

ARTICLE INFO

ABSTRACT

Long-period pulse-like strong ground motions were recorded near the Milun fault and caused serious building damages in the Hualien City during the main shock of the 2018 Hualien, Taiwan, earthquake. In this paper, questionnaire survey on feeling of shaking, indoor damages, structural, and nonstructural damages to high-rise reinforced concrete residential buildings were analyzed by three building groups according to the positions to the Milun fault and different site conditions. Relationships between the results of questionnaire survey on building damages and characteristics of strong ground motions were studied. Furthermore, a characterized seismic source model was proposed to elucidate the generation mechanism of near-fault long-period strong ground motions. In this model, a shallow strong motion generation area (SMGA7) in the south part of Milun fault with rise-time of 2.6 s contributed to the long-period pulse-like strong ground motions. Besides, a deep SMGA (SMGA8) under the SMGA7 with rise-time of 1.2 s also contributed to the strong ground motions. Using this model, strong ground motions at the sites of buildings for questionnaire survey were synthesized. Because of the directivity effects, amplitudes of ground motions were increased from north to south along the Milun fault, which can explain the serious building damages at the buildings located at the southwest to the Milun fault. The reasons of building damages were also examined from the aspect of predominant periods of ground sites and fundamental periods of buildings, which were extracted from microtremor measurement. Damages at the buildings located on the central part of the hanging wall with relatively good site condition were the lightest for almost all the surveyed items. Pulses with period in the range of 1 s–2 s which were generated by the SMGA8 and amplified by the near surface layers are considered to be responsible for building damages.

1. Introduction

At 23:50 (local time), on February 6th, 2018, an Mw 6.2 earthquake with a shallow hypocenter depth of about 6.31 km (Central Weather Bureau, Taiwan) struck the nearshore of Hualien region, which located on the eastern coast of Taiwan with high seismicity. Long-period pulse-like strong ground motions were recorded near the Milun fault with high density, the levels of which increased from north to south along the

Milun fault. Serious building damages happened along the Milun fault. All of the four collapsed buildings located near to the southern part of the Milun fault. Even in buildings that have not collapsed, interior damage such as furniture falling over and cracks in the wallpaper may have occurred [1,2], but these damages cannot be physically inspected from exterior survey. Furthermore, a building can be continuously used or not is not only determined by the damages to the structures but also affected by the indoor damages which related to the continuity of living.
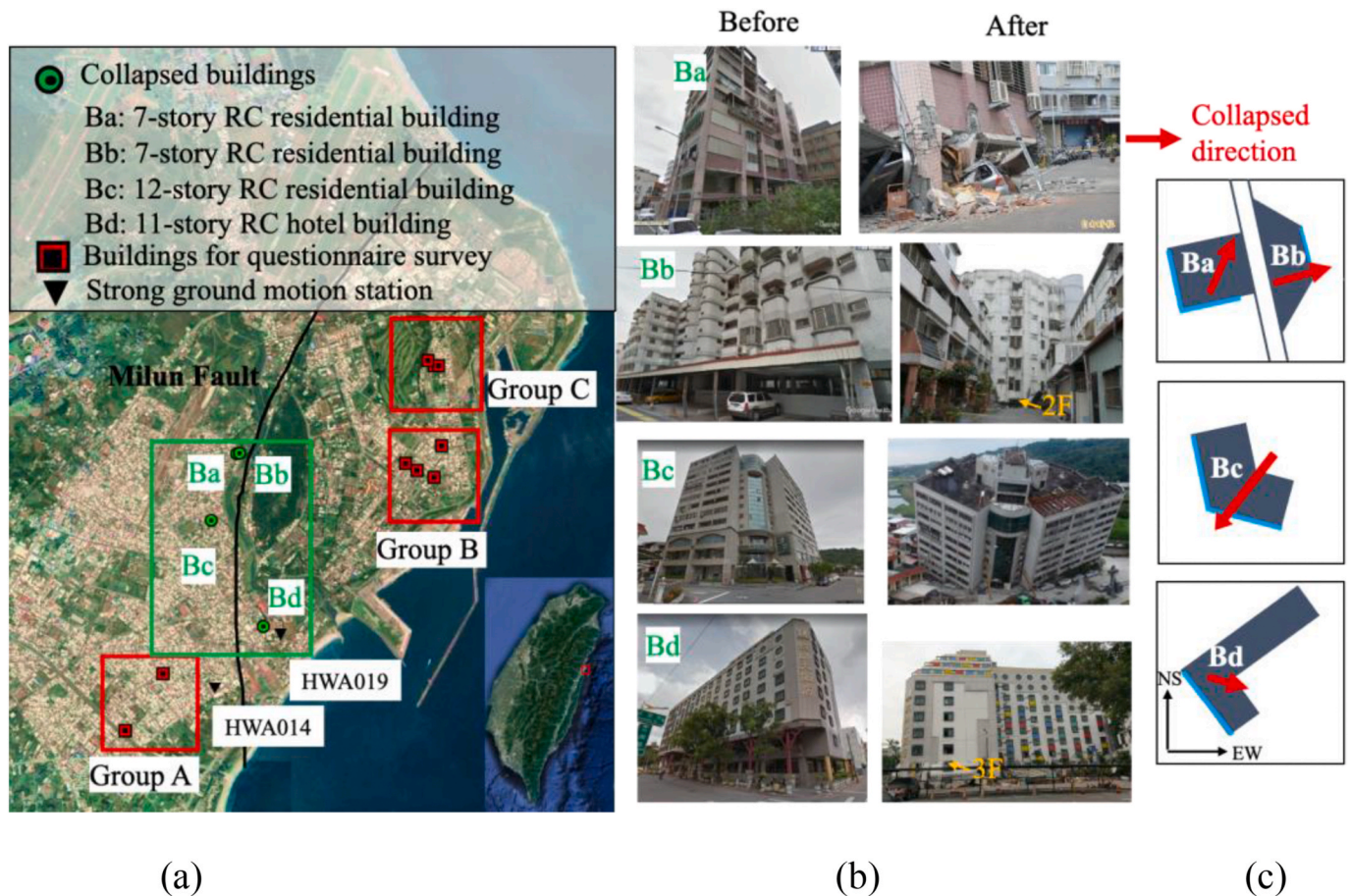
Fig. 1. (A) The area of Hualien City and the Milun fault are shown. The locations of collapsed buildings (Ba to Bd) are marked with green circles. The red squares indicate the locations of the buildings for questionnaire survey. (b) Photos of the four collapsed buildings before (from Google Earth) and after (from media) the earthquake. All of these four buildings were collapsed at lower stories. (c) Plane shapes of the collapsed buildings were descripted schematically. The facades shown in figure (b) for after the earthquake are marked with blue lines. The collapse directions are delineated with red arrows.

Though pulse-like strong ground motions were considered to be responsible for building damages [3,4], but the examination on relationships between characteristics of long-period pulse-like strong ground motions and structural/nonstructural damages and indoor damages is not enough.

Furthermore, the generation mechanism of the long-period pulse-like strong ground motions is complicated. From the moment tensor catalog published by U.S. Geological Survey (USGS), the 2018 Hualien earthquake was a left-lateral strike-slip fault with a high-dipping angle to the west. Similarly, the centroid moment tensor (CMT) indicates that this event had a mainly strike-slip focal mechanism with a minor thrust component dipping to the west. Moreover, according to the inversion results of source models [5–7] and locations of hypocenters of aftershock sequence [8], many researchers also insist that the seismogenic fault of this event was a steeply west-dipping fault. However, there is no well-known west-dipping fault in the subduction-collision transition zone offshore eastern Taiwan [9]. Source models of this seismogenic fault showed that only a minor slip was detected on the west-dipping fault [5,6]. There is a well-known active fault, the Milun fault, in the Hualien region running under the Hualien City. However, the Milun fault is a left-lateral reverse fault with a high dip angle toward the east [10–13], which is different from the results from the USGS and CMT. Therefore, many researchers insisted that the Milun fault was triggered by the west-dipping seismogenic fault as a passive event and the rupture of which mainly contributed to the generation of strong ground motions [5,6,14].

In this study, with the purpose to examine the damages of buildings

under the pulse-like strong ground motions, questionnaire surveys on indoor and structural/nonstructural damages were performed to nine reinforced concrete residential buildings. The answers of the questions were analyzed by three building groups according to positions to the Milun fault and site conditions. Furthermore, in order to elucidate the generation mechanism of near-fault long-period strong ground motions, a characterized seismic source model was proposed, which includes the west-dipping seismogenic fault, the Milun fault, as well as a part of the Lingding fault which is running at the south of the Milun fault and was also triggered. The strong ground motions at the sites of buildings for questionnaire survey were synthesized. Relationships between the different damage conditions at the three building groups with the characteristics of the synthesized strong ground motions were examined.

In this paper, firstly, the changes of characteristics of near-fault strong ground motions from north to south along the Milun fault on the footwall side and the hangingwall side were examined. Secondly, after the information of the target buildings and the application of the questionnaire survey were introduced, the analysis results and quantitative evaluation of the questions on feeling of shakings, indoor damages, nonstructural, and structural damages at buildings of each group were shown. Thirdly, the characterized seismic source model was proposed based on the inversion source model of Lee et al. [6]. The seismogenic structure of the Hualien area were briefly summarized and the ground structures of the strong ground motions stations were constructed. The synthetic ground motions at the sites of target buildings were generated using the Thin Layer Method. The relationships between
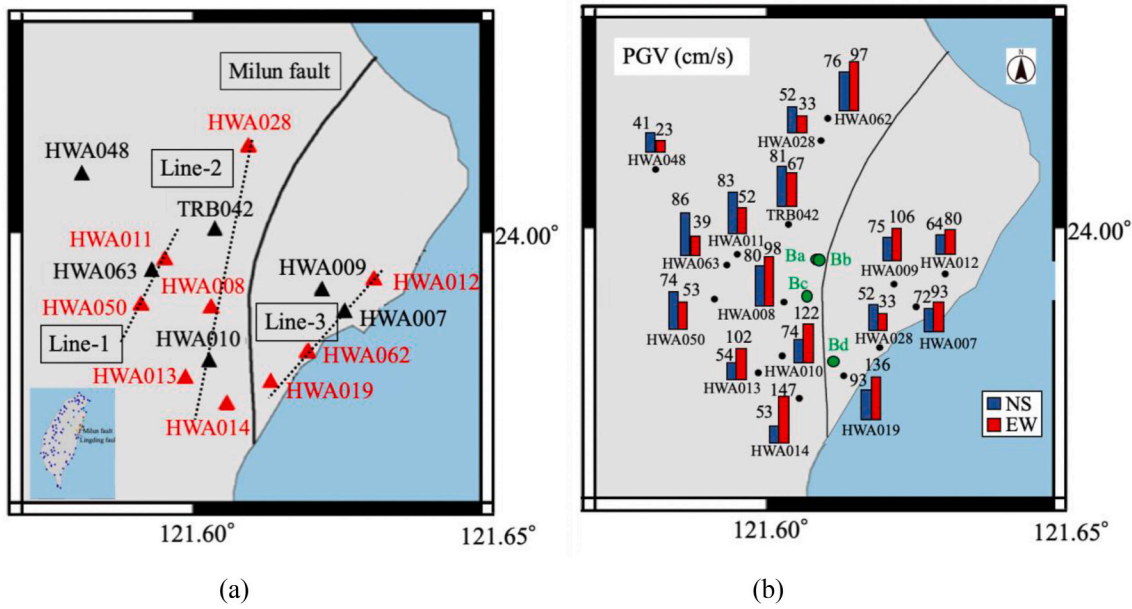
Fig. 2. (A) Locations of strong ground motion stations in the Hualien City (closed triangles). The red ones indicate the stations with ground structure data, whereas the black ones are without. The three dotted lines present the observation lines (Line-1 to Line-3). (b) The distribution of peak ground velocities (PGVs) in EW and NS direction.

building damages at each building groups and characteristics of synthetic strong ground motions were examined. Finally, the conclusions are presented.

2. Collapsed buildings and characteristics of strong ground motions

As shown in Fig. 1, the Milun fault is under the Hualien City running from northeast to southwest at the northern part and almost from north to south at the southern part. The collapsed buildings Ba to Bd located at the south part of the Milun fault. The collapsed buildings Ba and Bb were both 7-story reinforced concrete residential buildings, the lower stories

of which were totally collapsed. The building Bc was a 12-story reinforced concrete residential building with hotel rooms at the lower stories. Because of the collapse of the entrance hall, this building tilted to the southwest direction as shown by the arrow in the figure. The building Bd was a 11-story reinforced concrete hotel building, the lower two stories of which were totally collapsed. The collapsed directions are shown with red arrows. The locations of buildings for questionnaire survey are also shown in this figure, which will be explained in details in the next section.

Strong ground motion stations were installed in the Hualien City with high density, the locations of which are shown in Fig. 2. The changes of characteristics of strong ground motions from north to south
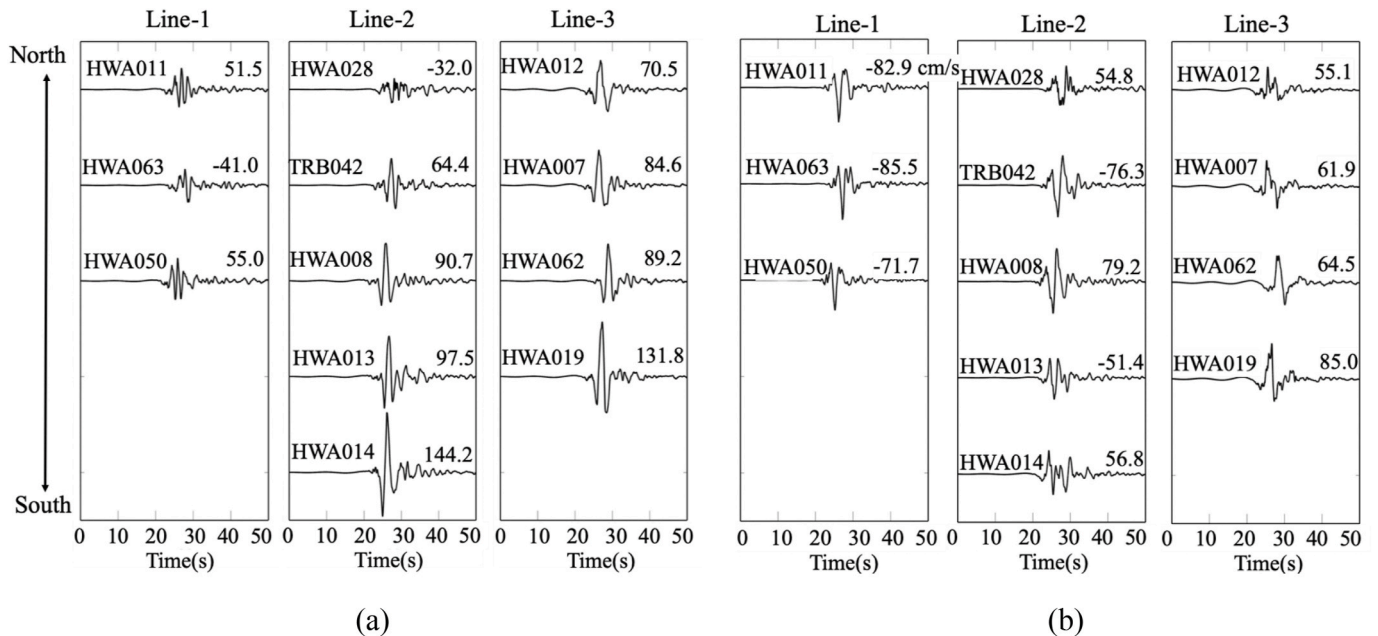

Fig. 3. Velocity time histories in the (a) EW direction and (b) NS direction at the stations of the three observation lines from north to south. The PGV (cm/s) of each waveform is noted.
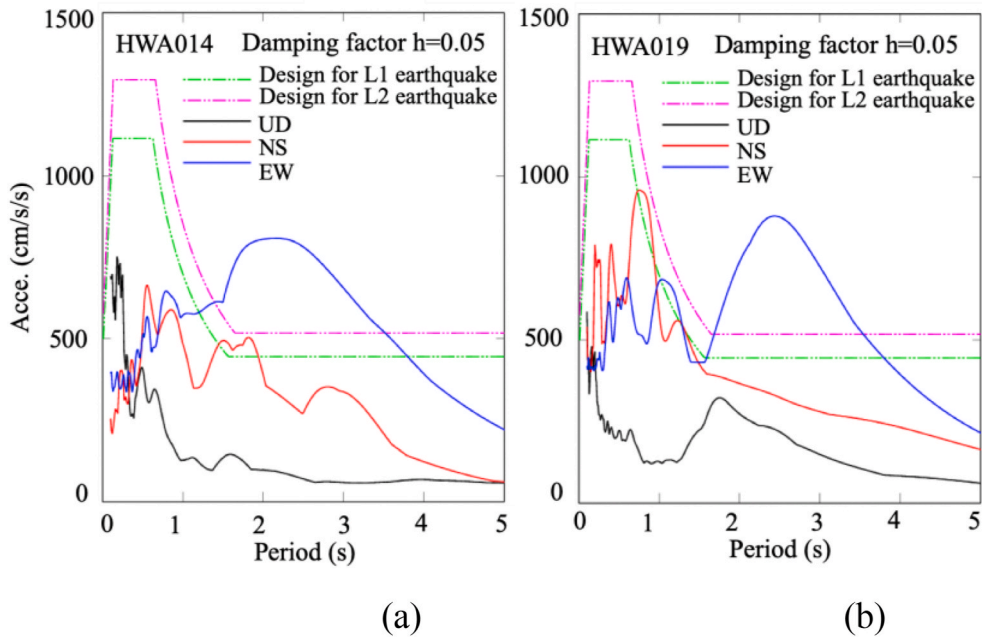
Fig. 4. Acceleration response spectra of records at the strong ground motion station (a) HWA014 and (b) HWA019. The spectra for level-1 (L1) and level-2 (L2) earthquake force in the aseismic design code of Taiwan were also shown.
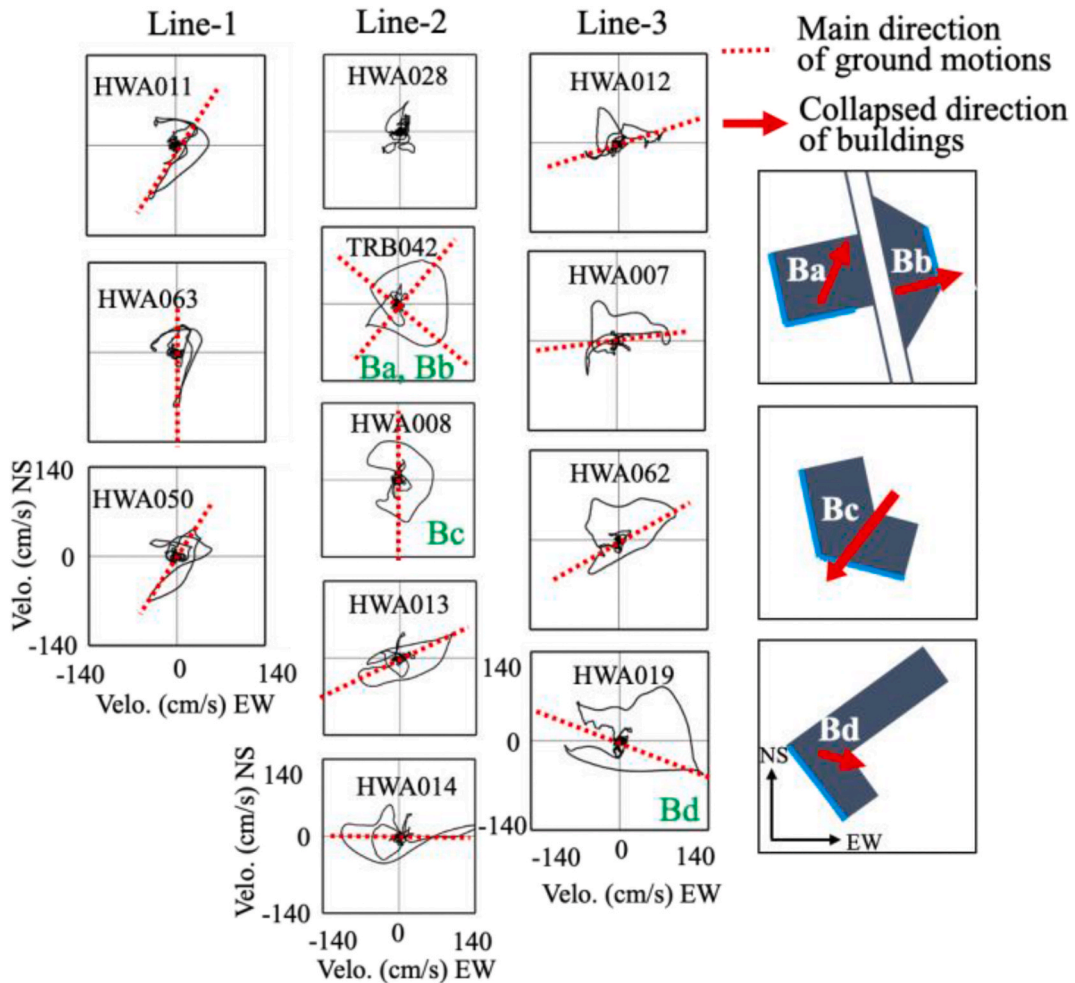

Fig. 5. Two-dimensional particle velocity orbits at stations of the three observation lines. The main directions in which the largest displacement happened are marked with broken red lines. The nearest station of the collapsed buildings is noted.
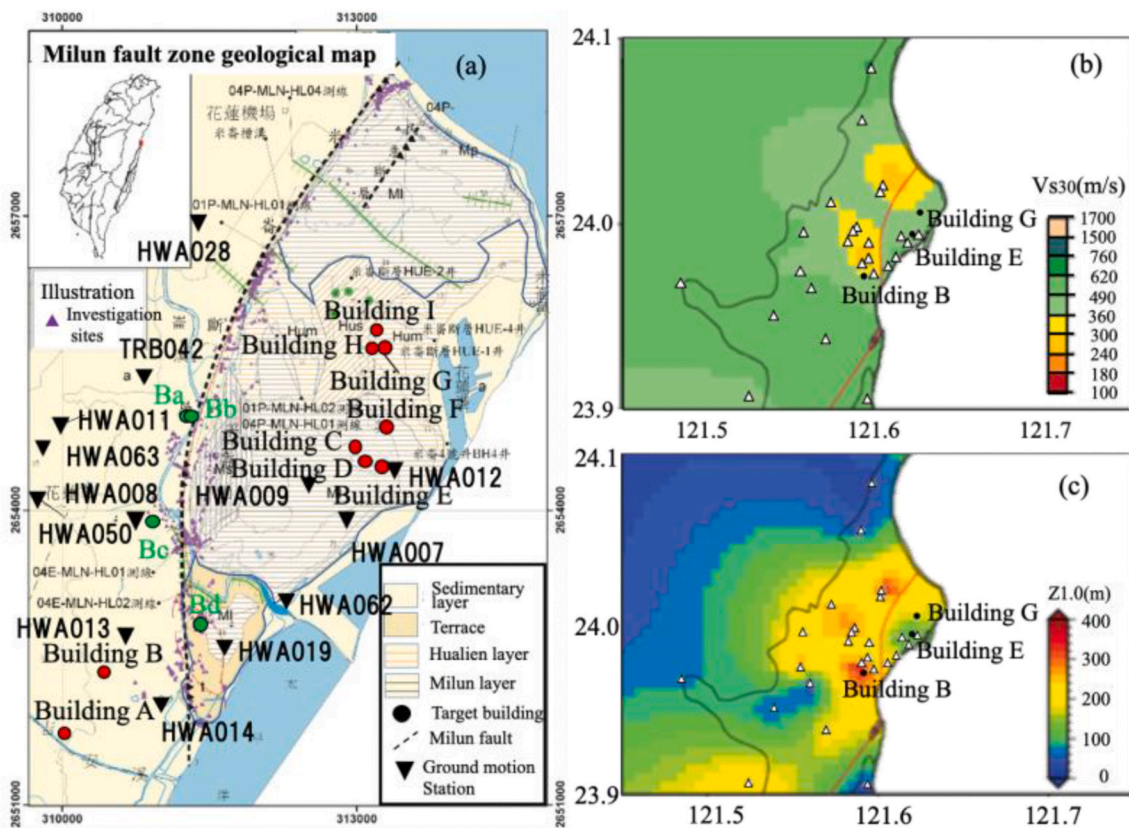
Fig. 6. (A) Distribution of buildings for questionnaire survey on the background of a geological map (Central Geological Survey, Taiwan). Different site conditions of the buildings for questionnaire survey can be seen from (b) the map of Vs_{30} and (c) the map of Z1.0 (the depth from the surface to the top of the layer with $Vs > 1$ km) which were published by Kuo et al. [15].

were examined based on three observation lines. The Line-1 and Line-2 are almost parallel to the Milun fault on the footwall side with distances from Milun fault about 1.7 km and 0.8 km, respectively. Because there are no stations at the northeast part of Hualien City, the Line-3 crosses the stations at the southeast side of Milun fault along the coast line. The peak ground velocities (PGVs) in EW and NS directions recorded at these stations are shown in Fig. 2(b). From Fig. 2(b), it can be visually determined that most of the blue bars (PGVs in NS direction) are higher than the red bars (PGVs in EW direction) on the north side of the Milun fault, while on the south side of the fault most of the red bars are higher than the blue bars. Therefore, generally, the PGVs in NS direction are larger than those in EW direction at the stations located near to the north part of the Milun fault, while at the stations near to the south part of the Milun fault the PGVs in the EW direction are larger than those in the NS direction.

The velocity waveforms along the three observation lines are shown in Fig. 3. Though there are no obvious pulse-like waves can be visually inspected from the velocity waveforms at stations of Line-1, long-period pulses indeed exist based on the quantitative identification [15]. From the velocity waveforms at stations of Line-2, long-period pulse-like waves can be seen obviously except from the waveforms of the station HWA028 which located at the northernmost of the Line-2. That is to say, with the rupture of Milun fault processed from north to south, the pulse-like waves were generated by the directivity effect and the amplitudes of which were increased. The largest PGV was recorded at station HWA014 with the value of 144.2 cm/s. At the Line-3, which is on the hanging wall of Milun fault, pulse-like waves also can be seen obviously. The amplitudes also increased from north to south.

Acceleration response spectra at strong ground motion stations HWA014 and HWA019, which located at the southernmost of the Milun fault on the footwall side and the hangingwall side, respectively, are

shown in Fig. 4. Comparing with the design spectra for level-1 (L1) input earthquake force (design earthquakes with recurrence interval of 475 yrs) and level-2 (L2) input earthquake force (maximum considered earthquakes with recurrence interval of 2500 yrs) in the aseismic design code of Taiwan, response accelerations in the period range of 2 s–3.5 s in the EW direction are much higher than the design levels.

Particle velocity orbits of the records at the three observation lines are shown in Fig. 5. Bow-shape particle displacement orbits of the stations at Line-1 are obvious, and the main movements of which are in the NS direction. As for the Line-2, displacements at the station HWA028 are small in both the NS and EW directions, and it is difficult to tell the main direction, i.e. in which direction the largest displacement happened. The particle displacement orbit at the station TRB042 is like a circle, the maximum displacements of which are almost the same in the northeast and southeast direction. At the station HWA008, the displacement in the NS direction is much larger than that in the EW direction. However, at the stations near the south part of Milun fault, i.e. HWA013 and HWA014, the displacements in the EW direction are much larger than those in the NS direction. That is to say the directions of main movements at the stations which are very close to the Milun fault on the footwall side changed from NS direction to EW direction. The main directions are marked with broken red lines. It can be seen that there is a close relationship between the collapsed directions of the buildings and the main directions of the strong ground motions.

Summarily, the gradual increase in the levels of strong ground motions from north to south toward the rupture direction of the Milun fault (i.e., directivity effect) is one of the reasons why the collapse of buildings is concentrated in the southern part of the Milun fault. Furthermore, according to the main directions of the strong ground motions and the collapse directions of buildings, the position to the Milun fault is also a factor to building damages. However, it is difficult to affirm the
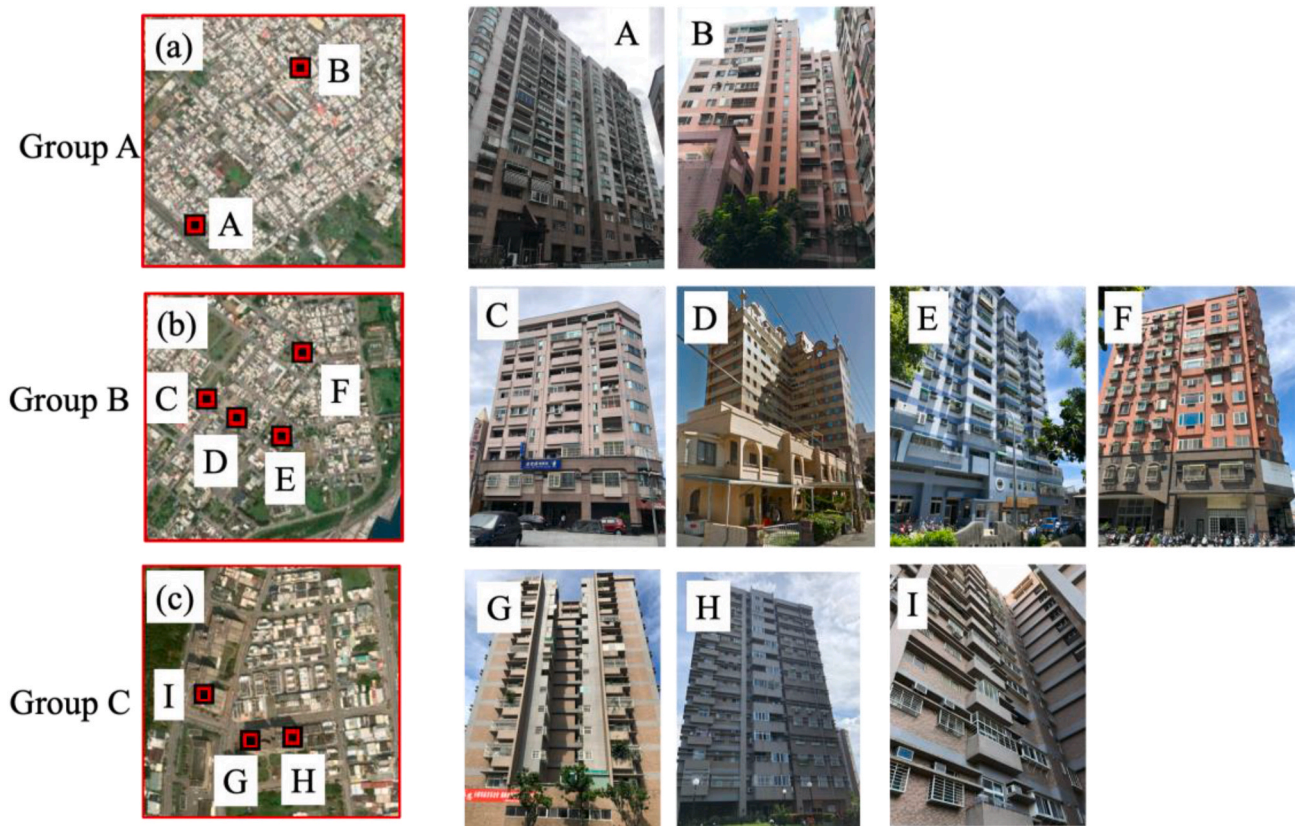
Fig. 7. Locations of the buildings for questionnaire survey in Group A to C. The appearances of the buildings of each group are shown beside.

relationship between high-level long-period strong ground motions with the building collapse, because the response characteristics of the collapsed buildings are unknown.

3. QUESTIONNAIRE survey on damages at residential buildings

3.1. Buildings for questionnaire survey

In this study, considering the characteristics of strong ground motions and differences in ground amplification characteristics, the buildings locate to the southwest of Milun fault, the central part and the northeast of the east side of Milun fault were selected. Questionnaire survey on feeling of shaking, indoor damages, nonstructural, and structural damages were performed to the residents of nine reinforced concrete residential buildings. Locations of the nine buildings are shown in Figs. 1 and 6(a) on the background of a geological map (Central Geological Survey, Taiwan). The Building A and B locate to the southwest of the Milun fault; Building C to F locate on the central part of the east side of the Milun fault; Building G to I locate to the northeast of the Milun fault.

From Fig. 6(a), it can be seen that the geological conditions on the east side and west side of the Milun fault are different. Distributions of Vs_{30} (average S-wave velocity of the surface soil from the ground surface to a depth of about 30 m) and Z1.0 (the depth from the surface to the top of the layer with Vs > 1 km/s, Vs: shear-wave velocity), which were published by Kuo et al. [15]; are shown in Fig. 6(b) and (c). The larger values of Vs30 and Z1.0 are, the less ground amplification effect to the seismic motions. From Fig. 6(a) it can be seen that the site conditions of the central part of the east side of the Milun fault are different with the around sites. Considering the different site conditions, answers of the questionnaire survey were analyzed in three groups, i.e. Group Ã C. In Group A, Building A and B locate at the sites with Vs_{30} in the range of 360 m/s to 490 m/s and Z1.0 of depth within 240 m–320 m. In Group B, Building C to F locate at the sites with Vs_{30} in the range of 300 m/s to 360 m/s and Z1.0 of depth within 80 m–160 m. In Group C, Building G to I locate at the sites with Vs_{30} in the range of 300 m/s to 490 m/s and Z1.0

Table 1
Information of buildings and the effective answers of questionnaire survey.

| Building	Structural Type	Year of Completion	Story Number	Number of Effective Answers	Story Range		
					Lower	Middle	Upper
					(Number of Effective answers)		
A	Reinforced concrete	1996	16	66	1F–5F (23)	6F–11F (28)	12F–16F (15)
B		1995	13	46	1F–4F (14)	5F–9F (18)	10F–13F (14)
C		2000	10	42	1F–3F (12)	4F–7F (17)	8F–10F (13)
D		2011	13	22	1F–4F (5)	5F–9F (11)	10F–13F (6)
E		1996	12	21	1F–4F (7)	5F–8F (11)	9F–12F (3)
F		1996	11	41	1F–4F (9)	5F–7F (16)	8F–11F (16)
G		2003	12	29	1F–4F (8)	5F–8F (9)	9F–12F (12)
H		2003	14	30	1F–5F (9)	6F–9F (6)	10F–14F (15)
I		2003	14	31	1F–5F (10)	6F–9F (8)	10F–14F (13)
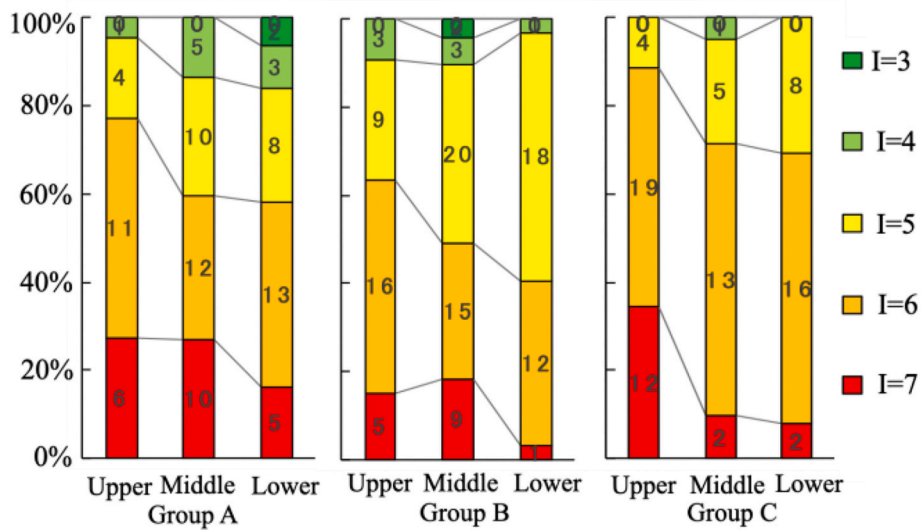
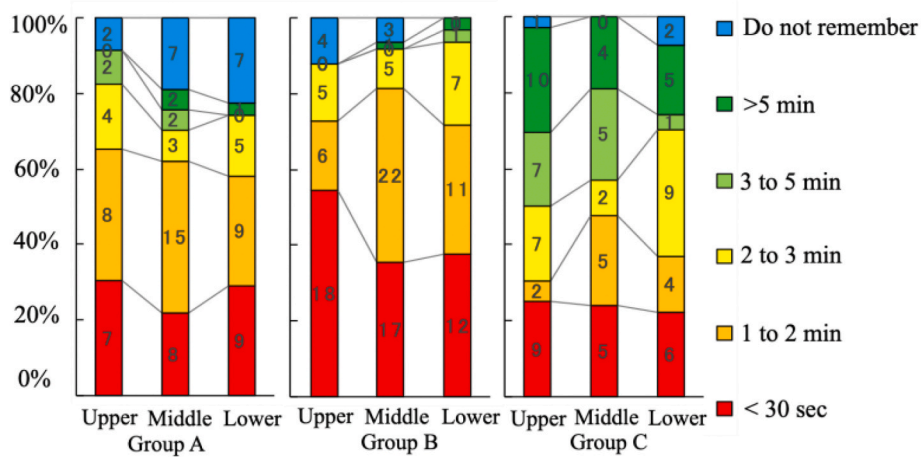Fig. 8. Seismic sensation intensity at buildings in each group.

Fig. 9. Duration of shaking at buildings in each group.

of depth within 160 m–200 m. It can be speculated that the site conditions of buildings in Group B are better than those of other two groups. Photos of the buildings in each group are shown in Fig. 7. Structural types, story numbers, and construction years of questionnaire survey of each building are tabulated in Table 1.

The questionnaire survey was performed in July 2018, almost 4 months after the earthquake. The papers of questionnaire survey were delivered to and collected from the residents through the managers of these buildings. The collection period of the questionnaire survey was almost one month. Totally, 328 effective answers were collected. The collection rate is about 82%. In order to examine the changes of building damages with the height, answers of questionnaire survey were analyzed according to the lower part, the middle part, and the upper part of the buildings. The numbers of effective answers of each building and those of each part are shown in Table 1.

3.2. Analysis results of questionnaire survey

3.2.1. Feeling of shaking

3.2.1.1. Seismic sensation intensity, duration; shaking types, hindrance to action; scared feeling. Analysis results of seismic sensation intensity are shown in Fig. 8. The sensation intensity scale is the same as the seismic
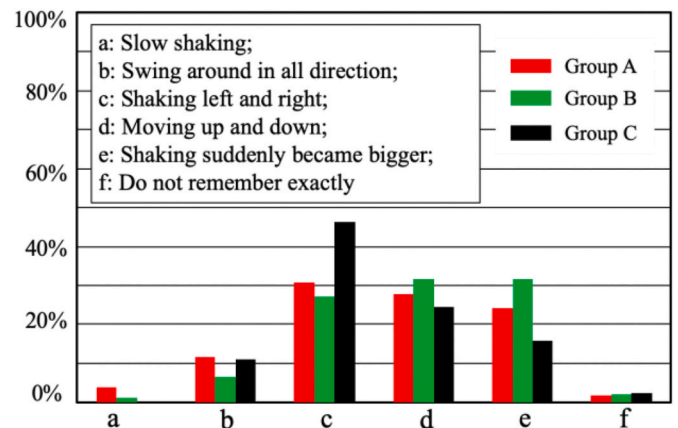

Fig. 10. Shaking types at buildings of Group A, Group B, and Group C.

intensity scale of Taiwan (the previous revision before 2020). It is found that the percentages of seismic sensation intensity of larger than 6 at buildings of Group C are higher than the values at the buildings of other two groups. The analysis results of shaking duration shown in Fig. 9. The
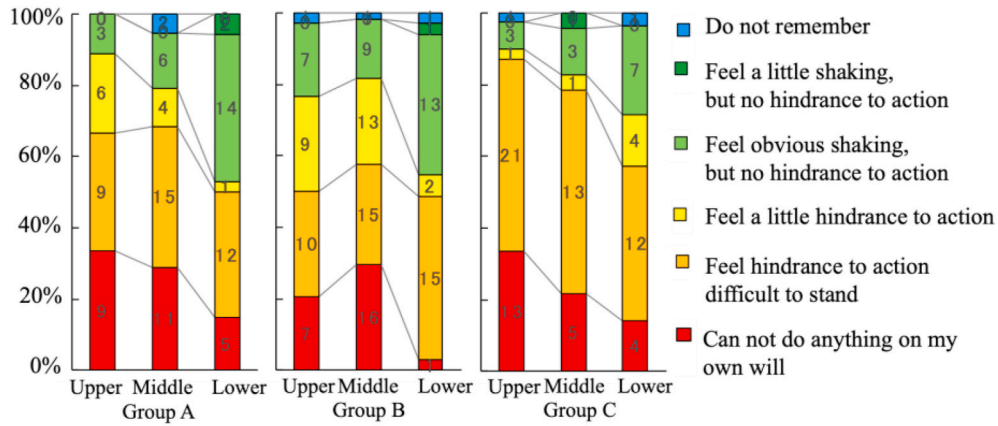
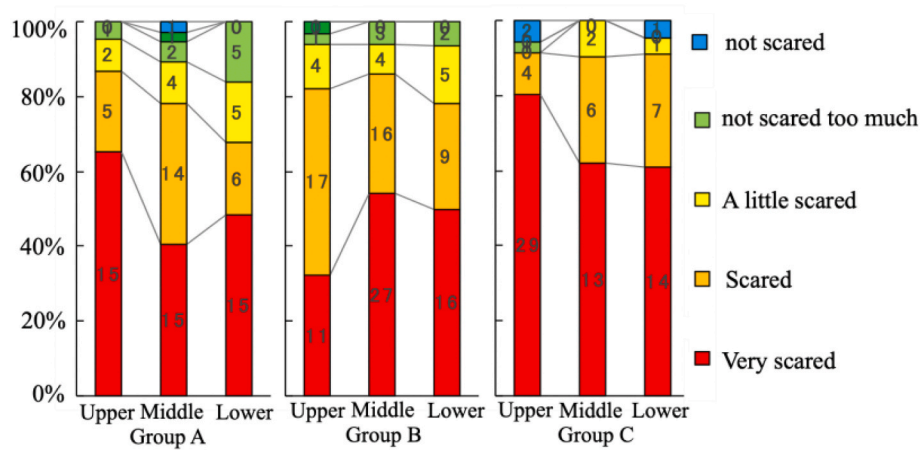**Fig. 11.** Hindrance to action at buildings in each group.

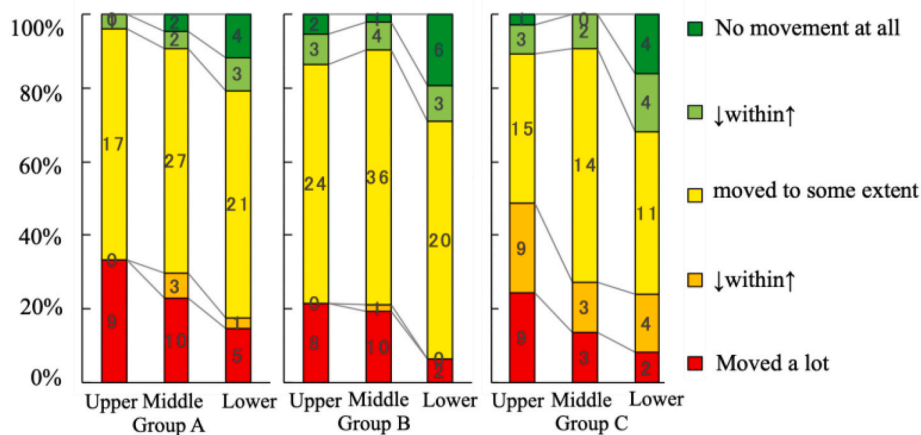**Fig. 12.** Scared feeling at t buildings in each group.

Fig. 13. Movement of big-size furniture at buildings in each group.

percentage of shaking duration of more than 3 min (above the yellow part) are the highest at the buildings of Group C. Besides, the shaking lasted longer at the upper stories than at the lower stories of the buildings of Group C. On contrast, for buildings of Group B, the percentages of shaking duration of less than 1 min are the largest among the three building groups. In Fig. 10, the results on the types of shaking are shown. It can be seen that the percentages of the shaking type c (shaking left and right), d (moving up and down), and e (shaking suddenly became bigger) are almost the same at the buildings of Group A and Group B. However, the percentage of the answers to shaking type c is much higher than other answers at the buildings of Group C. Analysis results on the hindrance to action at the buildings of each group are shown in Fig. 11. It can be seen that the percentages of feeling hindrance to action (orange and red bars) at the buildings of Group C are much higher than those at other building groups. And the percentage increases from lower stories to upper stories. From the results on the scared feeling as shown in
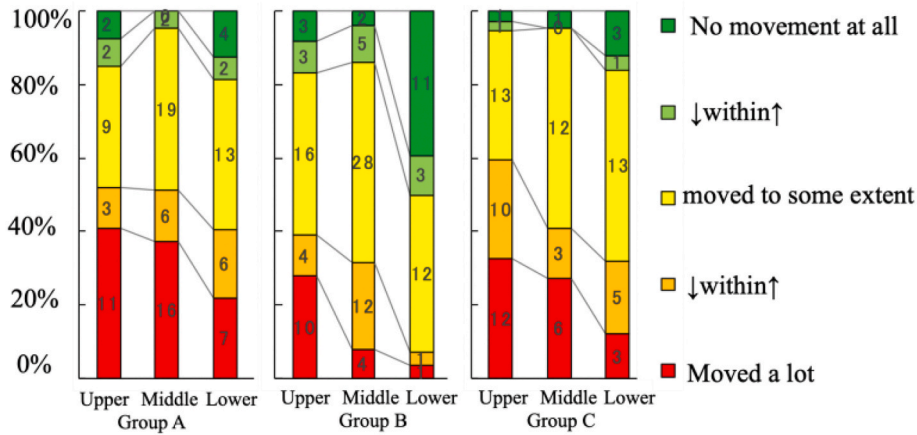
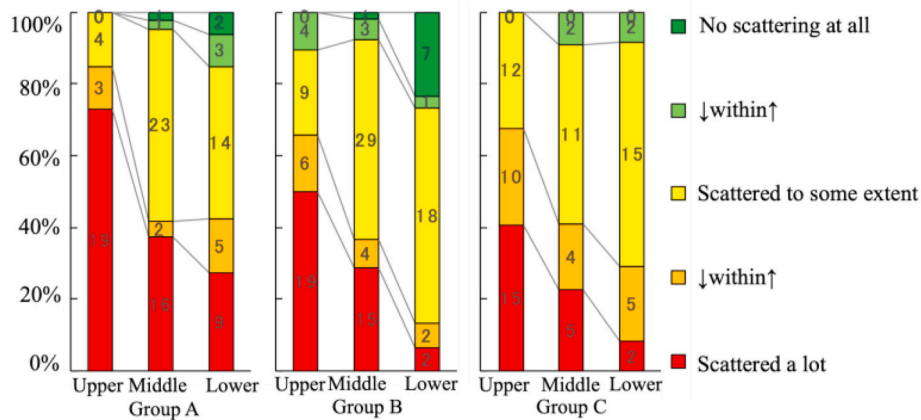**Fig. 14.** Movement of medium-size furniture at buildings in each group.

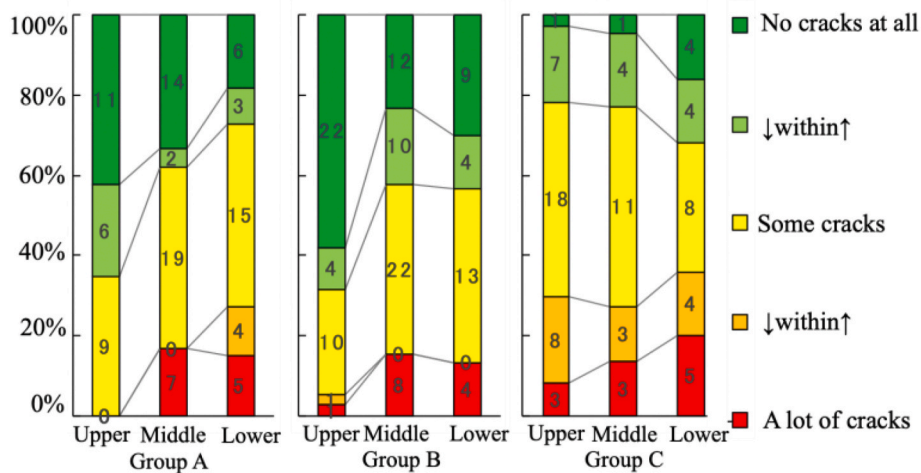**Fig. 15.** Scattering of small items at buildings in each group.

Fig. 16. Cracks in interior nonstructural walls of buildings in each group.

Fig. 12, it can be seen that the percentages of very scared at the buildings of Group C are the highest at each part of the buildings.

3.2.2. Indoor damages (movement of big- and medium-size furniture; scattering of small items)

Analysis results on the movement of big-size furniture (including the television tables, bookshelves, refrigerators, and so on) and medium-size furniture (including beds, tables, chairs, and so on) are shown in Figs. 13 and 14, respectively. It can be known that the percentages of answers to "moved a lot" increase from lower stories to upper stories at all buildings. The percentages of the answers to "moved a lot" and "within" (red and orange bars) are much higher at the buildings in Group C than at other buildings. On contrast, it can be known that the movements of big- and medium-size furniture were the lightest at the buildings of Group B.
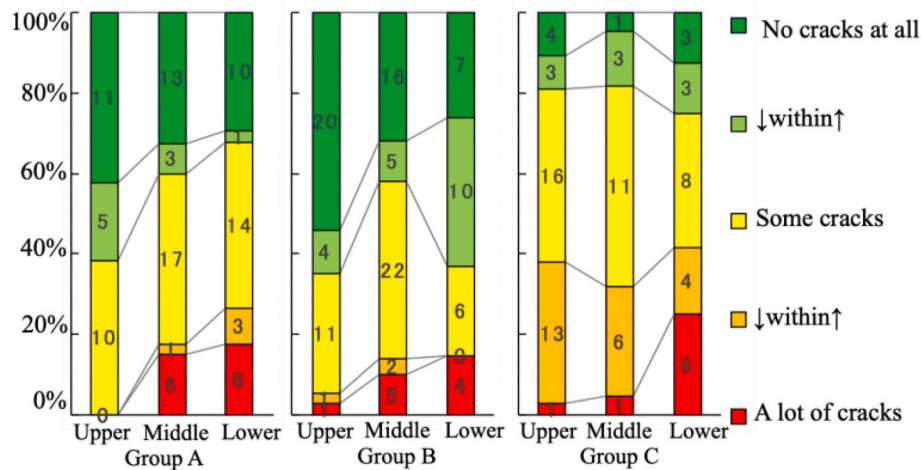
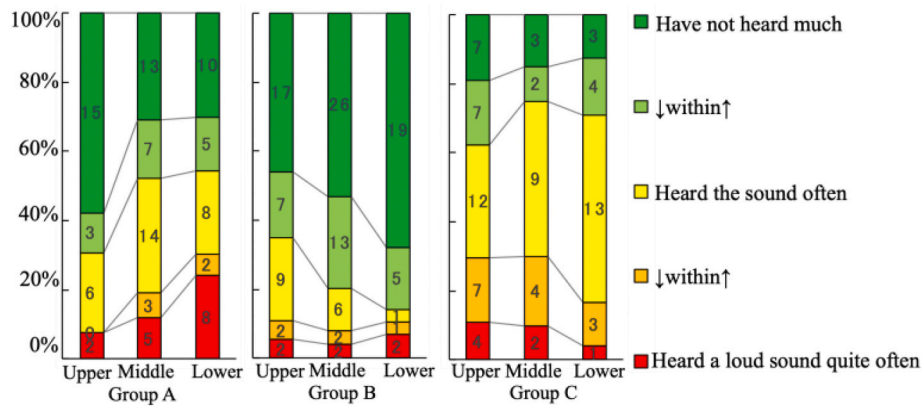**Fig. 17.** Cracks in concrete of structural members of buildings in each group.

Fig. 18. Hearing of sound of cracks at buildings in each group.

Table 2
Scores (S_i) for the choices of questions.

Questions		Hindrance to Action	Feeling Scared	Movement of furniture	Scattering of small items	Cracks in walls	Sound	Duration	Scores (S_i)
Choices	1	Cannot do anything on my own will	Very scared	Moved a lot	Scattered a lot	A lot of cracks	Heard loud sound quite often	>5 min	5
	2	Feel hindrance to action difficult to stand	Scared	within	within	within	within	3–5 min	4
	3	Feel a little hindrance to action	A little Scared	Moved to some extent	Scattered to some extent	Some cracks	Heard the sound often	2–3 min	3
	4	Feeling obvious shaking, but no hindrance to action	Not scared too much	within	within	within	within	1–2 min	2
	5	Feeling a little shaking but no hindrance to action	Not scared	No movement at all	No scattering at all	No cracks at all	Have not heard much	<30 s	1

Results on the scattering of small items are shown in Fig. 15. It can be seen that the percentages of answers to "scattered a lot" and "within" (red and orange bars) increase from lower stories to upper stories at all buildings. Scattering of small items happened severely in the buildings of Group A.

3.2.3. Damages to bodies of buildings (structural and nonstructural damages)

Analysis results on questions relating to damages to the bodies of buildings, including the cracks in interior nonstructural walls and cracks in concrete of structural members are shown in Figs. 16 and 17, respectively. The results on hearing of sound of cracks is shown in Fig. 18. It can be seen that, generally, the percentage of the answers to "a

lot of cracks" for both the cracks in interior nonstructural walls and concrete of structural members decrease from the lower stores to the upper stories. Moreover, the percentages of the answers to "a lot of cracks" and "within" (red and orange bars) at the buildings of Group C are much higher than at other buildings.

3.3. Quantitative evaluation of questionnaire survey results

In order to quantitatively examine the building damages in three groups, scores are given to the choices of questions as shown in Table 2. The small values of S_i correspond to light damages, whereas the large values indicate severe damage. The final score (S_f) of each question are calculated following Equation (1).
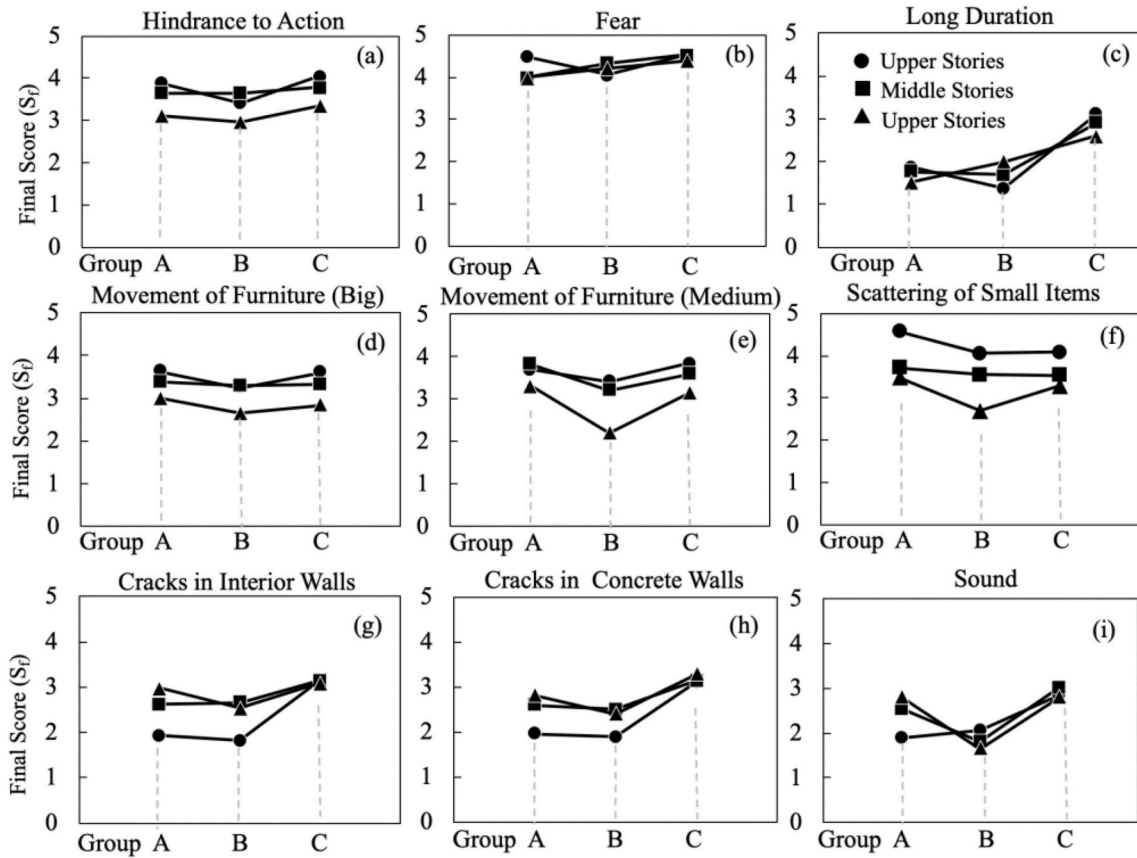
Fig. 19. The quantitative evaluation of damages with final scores (S_f) at buildings in each group.

$$S_f = \sum_{i=1}^{c} (S_i * N_i) \Big/ \sum_{i=1}^{c} N_i \qquad (1)$$

In where, i presents the ith choice of a question; c is the total number of choices of a question; N_i presents the number of answers to the ith choice of a question. For each question, the S_f was calculated at different height by counting the N_i according to the lower, middle, and upper stories. The results of S_f at different height of buildings in the three groups are shown in Fig. 19.

Based on the quantitative analysis results, the differences of damages at the buildings in each group can be read more easily. The values of S_f for Group B are the lowest for almost all the questions, excepting the values for the feeling of fear, which are almost the same at buildings in all groups. It can be known that almost all the damages are the lightest at the buildings of Group B. On contrast, the values of S_f relating to long duration and cracks in the bodies of buildings in Group C are obviously higher than the values of buildings in Group A. However, the values of S_f for scattering of small items are higher at the buildings in Group A than those at the buildings in Group C. Generally speaking, the higher the floor, the more serious the indoor damages. On the contrast, the lower the floor, the more sever the cracks in walls of buildings. For the buildings of Group C, cracks also occurred in the walls of higher stories.

4. Generation of near-fault pulse-like strong ground motions

4.1. Seismogenic structures

Taiwan is located on the convergent boundary between the Eurasian and Philippine Sea plates. The average velocity of the block motion of the Philippine Sea plate to the northwest direction is about 82 mm/yr [16]. The collision between these two plates causes very rapid uplift and develops a series of active faults in the east coastal range of Taiwan [5].

Also, the Eurasian plate is subducting eastward beneath the Philippine Sea plate in southern Taiwan, whereas the Philippine Sea plate is subducting northwestward beneath the Eurasian plate along the Ryukyu trench in northeastern offshore of Taiwan [8,9]. However, the tectonics from the western end of the Ryukyu trench to northeast offshore Taiwan is still controversial [6]. The seismogenic fault, a steeply west-dipping fault with strikes of 208°–220° [17], is considered as a part of the controversial region near or/and under the Hualien City. Lee et al. [6] insisted that there is a coastal range bedrock under the coastal range. The north-south striking west-dipping fault is the boundary fault between the coastal range and central range and the boundary between the coastal range bedrock and shallow Longitudinal Valley sediments.

The Longitudinal Valley of eastern Taiwan is the suture zone between the Philippine Sea Plate and the Eurasian plate. Hualien City is located on the northernmost of the Longitudinal Valley, at the transition from collision to subduction, which results in complex seismogenic structures [8,13,18–20]. In this region, destructive earthquakes occurred frequently with recurrence interval of as short as 70 yrs [4,13] due to the Milun fault, which is an active inland fault related to the Mw 7.3 Hualien earthquake in 1951 [13,21,22] as well as the Mw 6.2 Hualien earthquake in 1986 [23,24]. Based on the investigation of building damages and surface ruptures along the Milun fault [14,24,25] and seismogenic deformation of the Hualien region [26,27], the Milun fault was considered to be the main strong ground motion generation area.

Moreover, the Lingding fault, which is an east-dipping fault in the northernmost of Longitudinal Valley [13], was also active. Apparent breaks and damages of the Hualien Bridge were found close to the northern end of the Lingding fault [6,15,25]. Because the Milun fault does not extend southwards into the Longitudinal Valley [28], the Lingding fault and the Milun fault are independent. Though the seismogenic tectonic of this region is still challenging, the presence of the
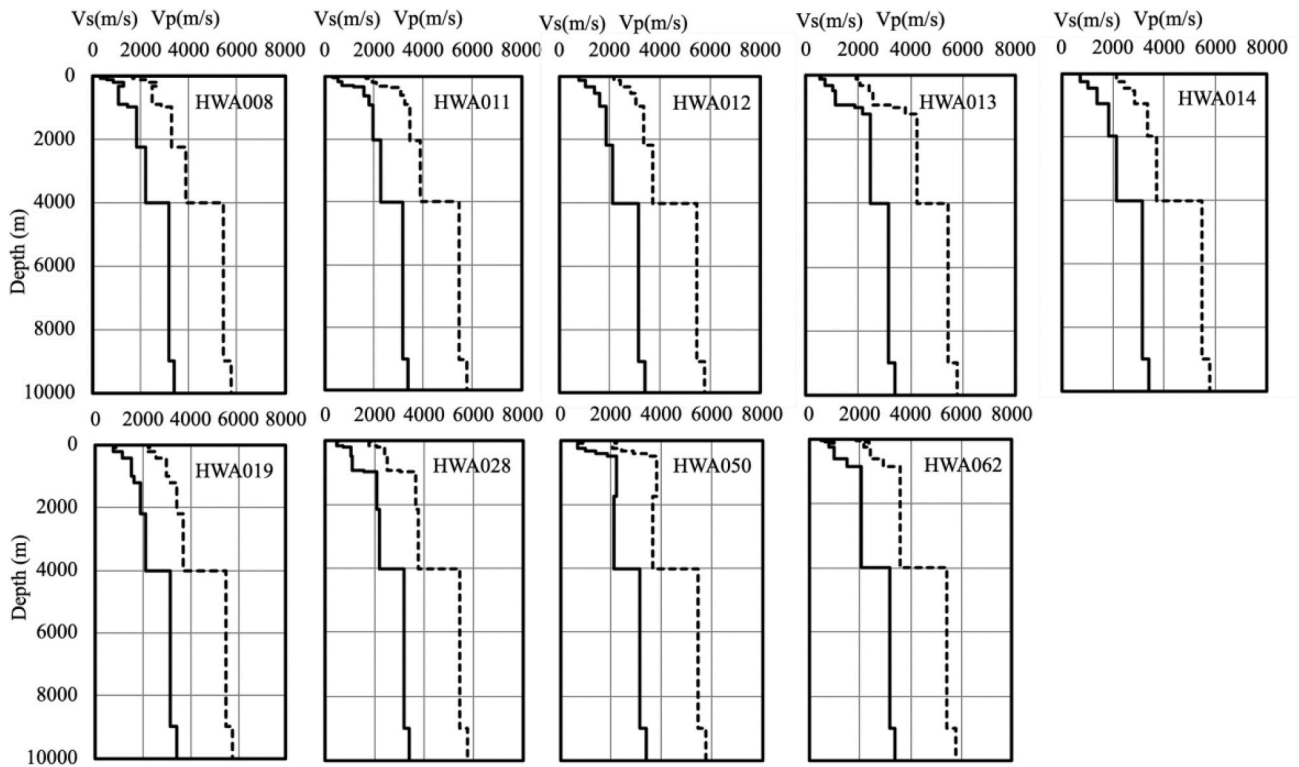
Fig. 20. Ground structures at the sites of strong ground motion stations combing the data from NCREE for the shallow part with depth <4 km and the data from CWB for the deep part with depth >4 km.

west-dipping Milun faults is unambiguous. Milun fault and the Lingding fault were triggered by the west-dipping fault as passive events.

4.2. Ground structures at strong ground motion stations

The Hualien City sits on Holocene alluvial deposits [14,29,30], but the geological conditions of the ground surface on the east (hanging wall) and west (foot wall) side of Milun fault are different [31]. The ground surface of the west side is a sediment layer, whereas the east side is called the Milun table land, which is composed of terrace, Milun layer,

and the Hualien layer. The Milun layer has relatively higher shear-wave velocity and shallower depth.

In this study, ground structures at the sites of ground motion stations near the Milun fault were constructed by combing the data from National Center for Research on Earthquake Engineering (NCREE) for the shallow part with depth of less than 4 km and the data from CWB (Central Weather Bureau, Taiwan) for the deep part with depth of more than 4 km. Because the limitation of data base, not all of the ground structures of the sites of ground motion stations can be constructed. The stations with and without ground structure data are shown in Fig. 2(a) as
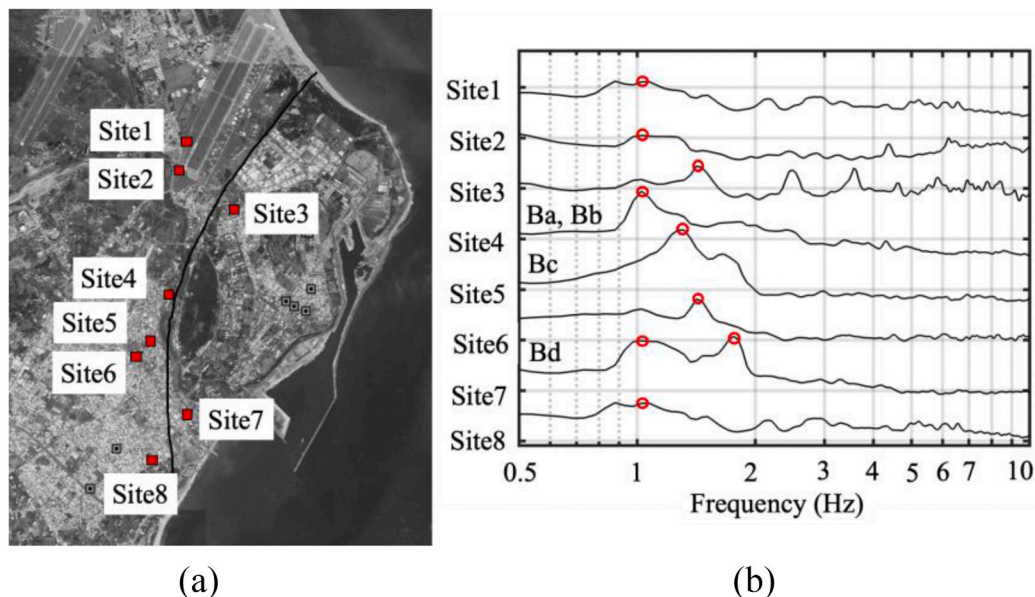

(a)   (b)

Fig. 21. (A) The ground sites at where ambient noise have been measured; (b) H/V spectra at the sites. The peaks of the spectra are marked with open red circles.
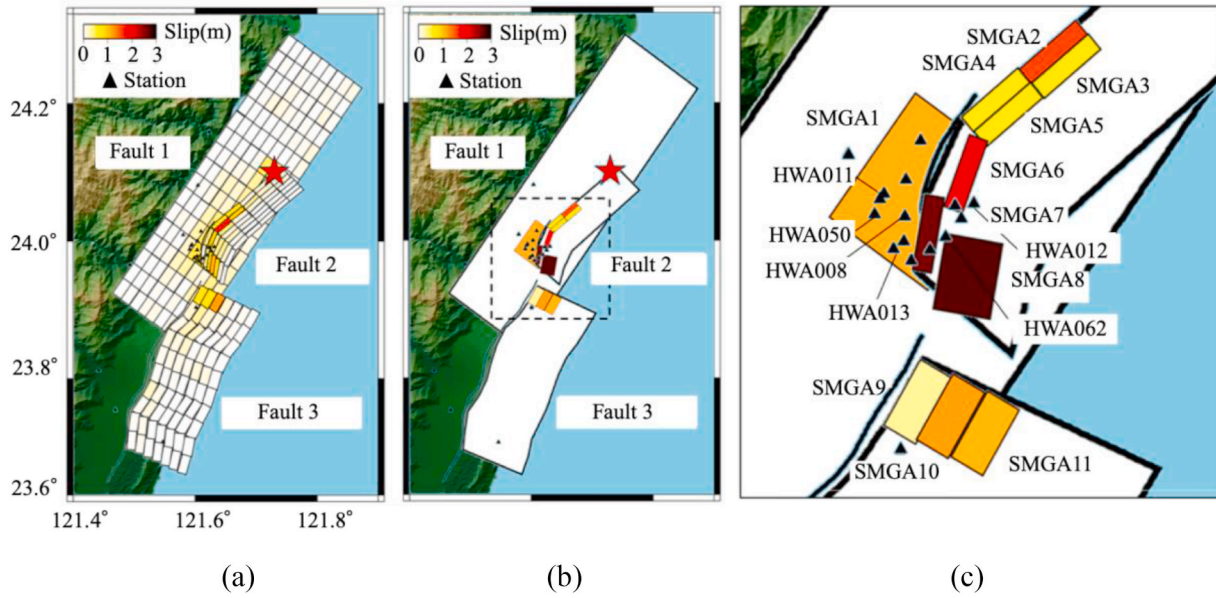
Fig. 22. (A) Slip distribution on the Fault 1 to Fault 3 [6]; (b) Characterized source model; (c) A zoom-up figure of the main part of the model.

red triangles and black triangles, respectively. P-wave velocity (Vp) was calculated from S-wave velocity (Vs) based on the relationship proposed by Kitsunezaki et al. [32] as shown in Equation (2). Density ρ was determined based its relationship with Vp, which was proposed by Gardner et al. [33]; as shown in Equation (3). Quality factor Q was determined following Equation (4).

$$Vp(\leq 3500m/s) = 1.11Vs + 1290$$
$$Vp(\geq 3500m/s) = \sqrt{3}Vs \qquad (2)$$

$$\rho = 0.31Vp^{1/4} \qquad (3)$$

$$Q = Vs/15 \qquad (4)$$

The S-wave and P-wave velocity profiles of all the stations with ground structure data are shown in Fig. 20. For the sites with no ground structure data, the data of the nearest station were used to synthesize strong ground motions.

Ambient noise at eigth ground sites along the Milun fault from the north to south were measured. The sites for ground ambient noise measurement were selected as the site of seismic observation station or the site of damaged buildings. The H/V spectra of the ambient noise were examined. The measured sites and the H/V spectra are shown in Fig. 21. The Site 4, 5, and 7 are on the sites of collapsed buildings. Other sites are close to strong ground motion stations. From H/V spectra it can be seen that the predominant frequencies of almost all of the sites are in the frequency range of 1 Hz–2 Hz.

4.3. Characterized seismic source model

Inversion source models of the 2018 Hualien earthquake have been proposed by many researchers [5–7]. Yang et al. [5] estimated the fault model using ascending and descending InSAR (Interferometric Synthetic Aperture Radar) deformations derived from ALOS-2 and Sentinel-1 satellite SAR images, and GPS displacements. Wen et al. [7] interpreted the rupture properties of the 2018 Hualien earthquake by inverting teleseismic body wave and forward modeling GPS coseismic deformation. To investigate the rupture properties, Lee et al. [6] performed the joint source inversion combing teleseismic body waves, local ground-motion waveforms, and Global Positioning System (GPS) coseismic displacements. Based on the results of this joint source inversion, they suggested that the rupture started from the west-dipping fault plane (Fault 1) progressing from north to south, then triggered the slip on the Milun Fault (Fault 2) and the Lingding Fault (Fault 3), successively. In this study, we focus on the generation mechanism of the near-fault long-period ground motions. Therefore, Lee's model was used to construct the characterized source mode of the 2018 Hualien earthquake.

The displacement distribution of Lee's model is shown in Fig. 22(a). The areas with large displacement correspond to the strong ground motion generation areas (SGMAs). The characterized source model was constructed as shown in Fig. 22(b). Geometry parameters of SMGAs were determined through the searching and calibration of best-fitting fault geometry parameters. As a result, eleven SMGAs (SMGA1 to SMGA11) were determined, parameters of that are listed in Table 3. Displacements on the background are not considered. The rake angles,

Table 3
Parameters of SMGAs in the characterized seismic source model.

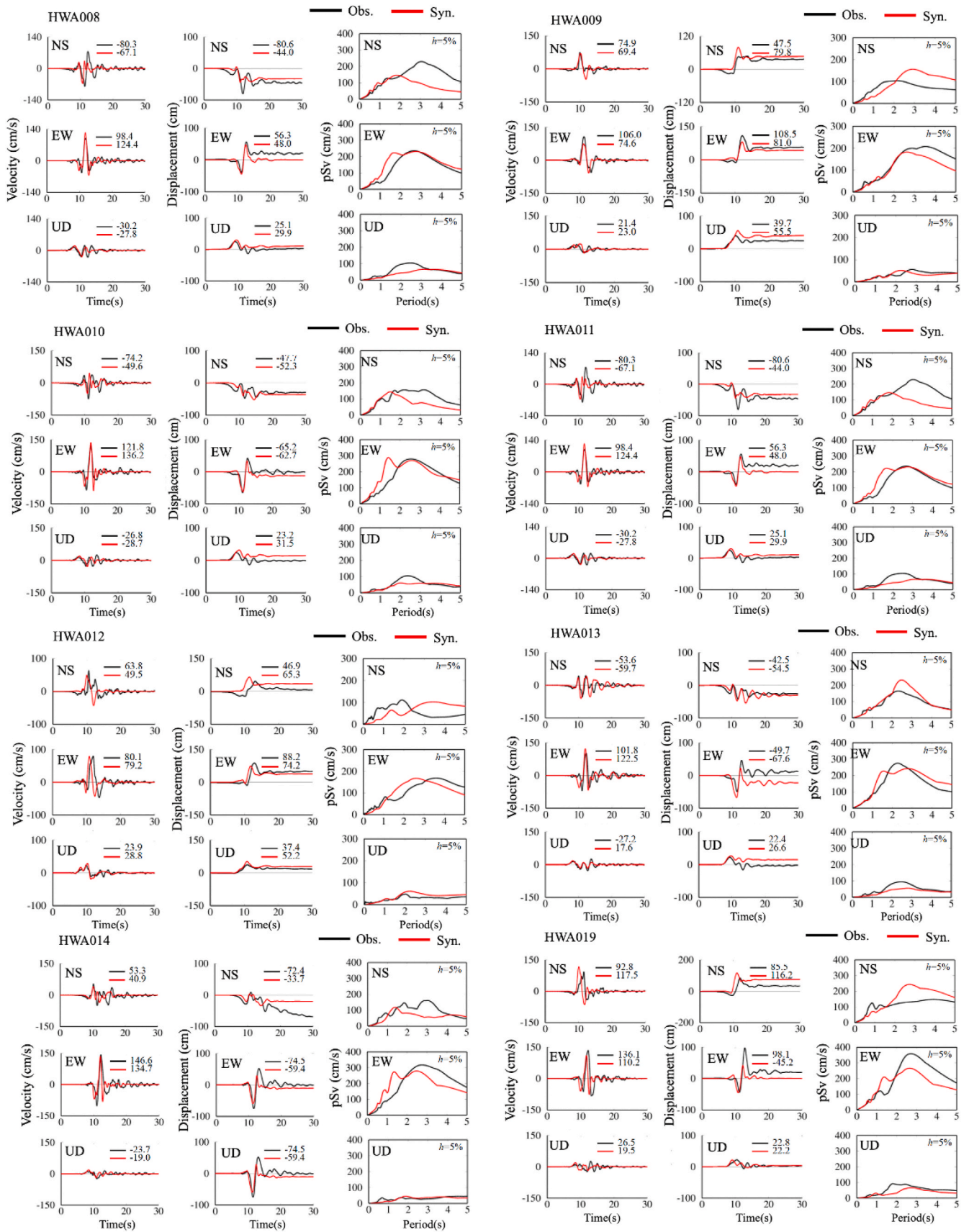| Fault	Fault 1	Fault 2							Fault 3		
SMGA	1	2	3	4	5	6	7	8	9	10	11
Length(m)	6	3	3	3	3	3	3	3	3	3	3
Width(m)	9	3	3	3	3	3	3	9	3	3	3
Rake Angle	215.7°	50°				20°	10°	10°	30°		
Dip Angle	56.4°(W)	75°(E)							60°(E)		
Slip Angle	70°	50°	50°	20°	20°	0°	0°	70°	0°	45°	60°
Slip(m)	1.1	1.6	0.7	0.7	0.7	2.0	2.6	2.7	0.3	1.2	1.1
Rise Time(s)	1.6	1.2	1.2	1.2	1.2	2.0	2.6	1.2	0.6	0.6	0.6
Rupture Velocity(km/s)	3.0	2.0									
$M_0(\times 10^{17}Nm)$	15.8	3.83	1.67	1.67	1.67	4.78	6.22	20.8	0.717	2.87	2.63

Fig. 23. Comparison of velocity waveforms, displacement waveforms, and pseudo velocity response spectra (pSv) between the synthesized results (red lines) and the observed records (black lines) at near-fault strong ground motion stations.
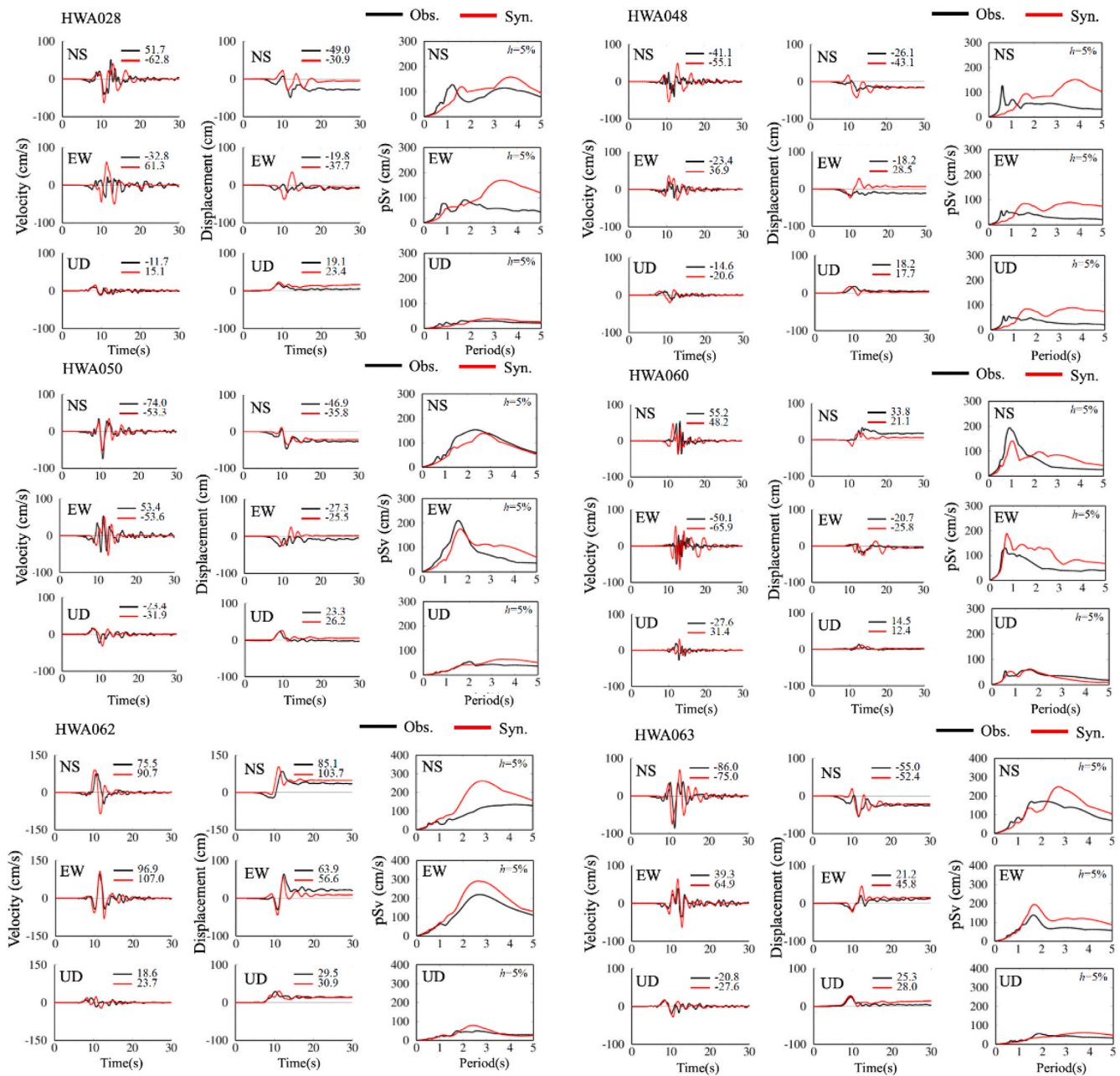
Fig. 23. (*continued*).

dip angles, and rupture velocities of the three faults are similar to those of Lee's model. A zoom-up figure of the main part of the model is shown in Fig. 22(c). The main energy generation areas are SMGA7 and SMGA8 on the Milun fault, the maximum slips of which reached to 2.6 m and 2.7 m, respectively. The SMGA7 correspond to the significant surface rupture trace along the Milun Fault in the field investigation [14,24,25]. The rise time of the source time functions of the SMGA6 and SMGA7 is set to be 2.0 s and 2.6 s, respectively, which correspond to long-period ground motions.

4.4. Synthesized strong ground motions

In this study, the Thin Layer Method (TLM) was used to perform simulation calculation of strong ground motions. TLM is an efficient semi-analytical method for the calculation of the fundamental solutions for layered media. The feasibility of TLM to numerical ground motion analysis has been demonstrated [34,35]. In the TLM, vertical

displacement is expressed in terms of a finite element expansion, while the horizontal displacement is numerically calculated based on the normal-modes method. The normal modes are obtained directly from the solution of two algebraic eigenvalue problems. Therefore, it is possible to accurately compute the displacement field not only in the far-distant field, but also at sites which are close to the source fault. Another advantage of this method is that once eigenvalues and modes of Rayleigh- and Love-wave equations have been obtained, the calculation of the complex rupture process including enormous combinations of source and receive points in a large seismic fault plane and soil model with complex vertical heterogeneity is possible. The methodology of TLM is out of the scope of this paper. Development and details of TLM can be found in many articles (e.g., Refs. [34,36–39].

In Fig. 23, the synthesized results on velocity waveforms, displacement waveforms, and pseudo velocity response spectra (pSv) at the near-fault ground motion stations are compared with those from the observed records. The displacement waveforms were obtained by integrating the
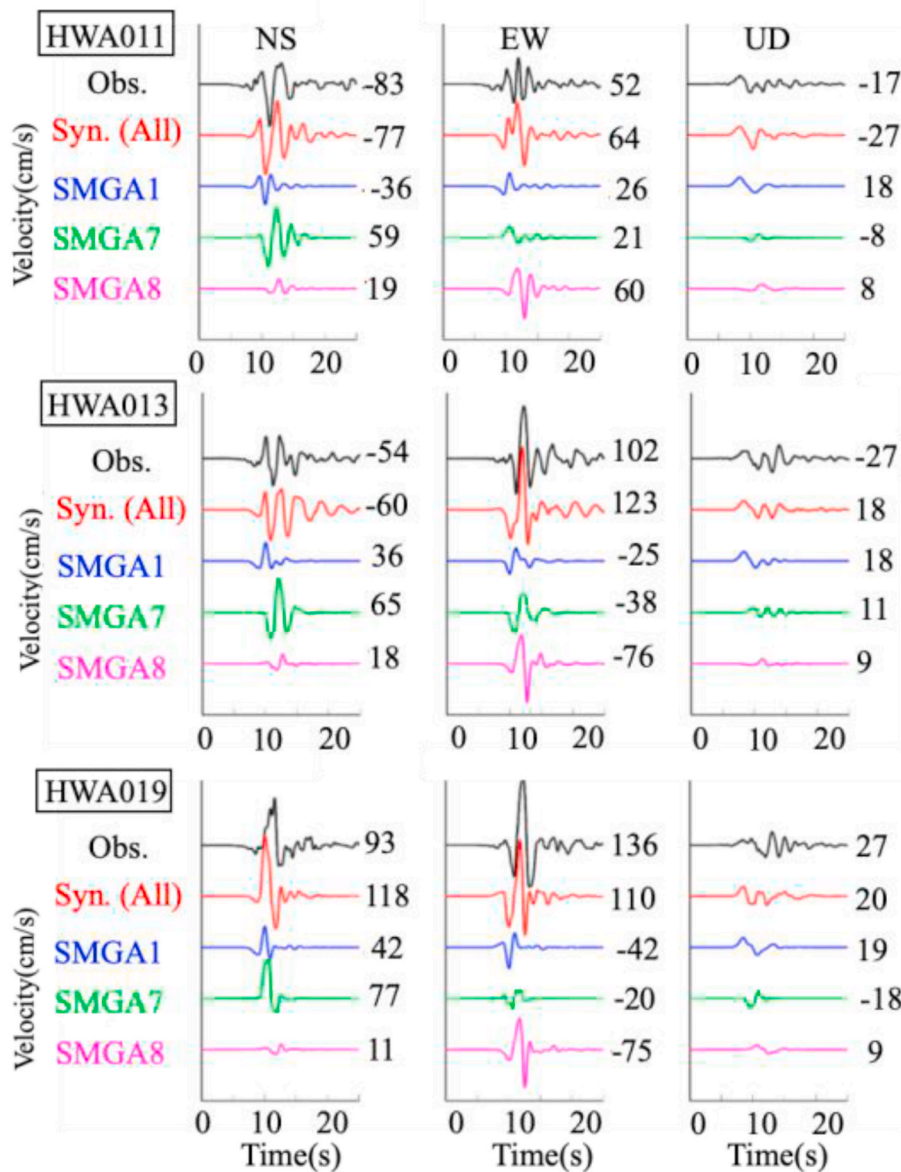
Fig. 24. Contribution of SMGA1, SMGA7, and SMGA8 to the generation of strong ground motions at the stations HWA011, HWA013, and HWA019.

velocity waveforms after the baseline correction. Effective frequency range of the numerical calculation model is < 2 Hz. It can be seen that the observed ground motions were well reproduced.

The contributions of main SMGAs to generation of strong ground motions at stations HWA011, HWA013, and HWA019 are shown in Fig. 24. It can be seen that the SMGA7 mainly contribute to the generation of pulse-like velocities in NS direction, while the pulses in the EW direction were mainly generated by the SMGA8. The velocities in the UD direction were due to the thrust movement of the SMGA1.

4.5. Relationship between synthesized strong ground motions and building damages

Strong ground motions at the sites of buildings for questionnaire survey were synthesized based on the proposed characterized seismic source model. Because there is no ground structure data at the sites of these buildings, the data at the sites of nearest ground motion stations were used. The ground structure data at station HWA013 was used to calculate the strong ground motions at the sites of buildings of Group A. The data at station HWA012 was used for buildings of Group B and

Group C.

The synthesized velocity waveforms and pSv at the sites of Building A, C, and G, as examples for each group, are shown in Fig. 25(a). Pulse-like ground motions in the velocity waveforms in both the EW and NS directions can be seen. The values of PGVs are compared in Fig. 25(b). It can be known that the PGVs at the site of Building A is much higher than those at the sites of other two buildings. PGVs in the UD direction are almost the same. Besides, the PGVs at the sites of Building C and G are almost the same. Pseudo velocity response spectra (pSv) are shown in Fig. 25(c). Peaks of pSv are marked with black triangles. It can be seen that the predominant periods at the site of Building A and G are in the range of 1 s to 2s, while the values at the site of Building C are in the range of 2 s to 3s. The predominant periods in the range of <2 s are due to the site effects. While, the predominant periods in the range of >2 s are considered to be generated by the long-period SMGAs (SMGA6 and SMGA7) of the Milun fault. In Fig. 25(c), the predominant periods (T_0) and maximum pSv (pSv_{max}) corresponding to the peaks are compared. The values of pSv_{max} are the highest at the site of Building A and lowest at the site of Building G.

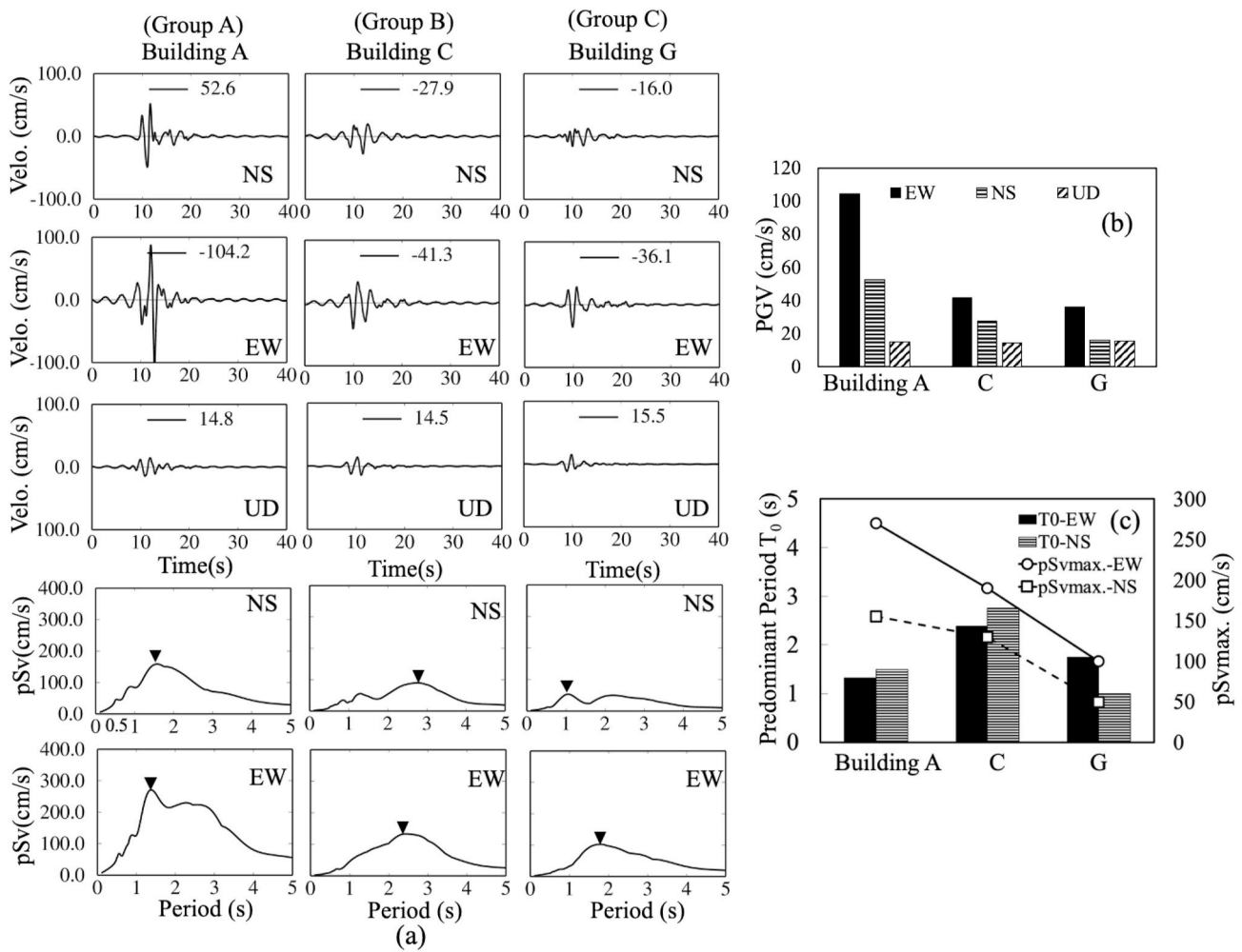Ambient noise at the top and the base of the buildings for

Fig. 25. (A) Synthesized velocity waveforms and pseudo velocity response spectra (pSv) at the sites of the Building A, C, and G. The peaks at the predominant periods are marked with triangles; (b) PGVs at the sites of Building A, C, and G; (c) predominant periods in the pSv and the corresponding maximum values of pSv (pSvmax.).
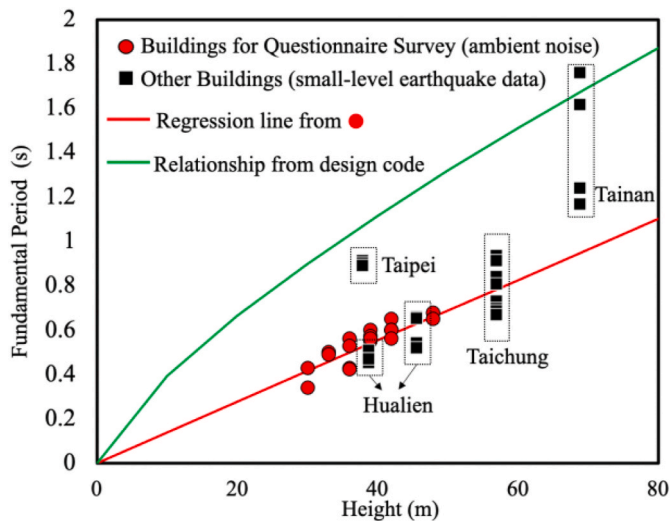

Fig. 26. Relationship between the heights and fundamental periods (in longitudinal and transvers directions) of buildings for questionnaire survey (closed red circles) and other buildings (closed black squares) located at Hualien and some other cities. The red line presents the regression relationship of the buildings for questionnaire survey. The relationship from aseismic design code of reinforced concrete buildings in Taiwan is shown in a green line.

questionnaire survey were measured. The fundamental periods of these buildings were obtained from the transfer functions between the top and the base of the buildings. The obtained linear relationship between building height and fundamental periods T of these buildings is shown in Fig. 26 with a red line [40]. The heights of the surveyed buildings are calculated by multiplying the story number with the story height, which is assumed to be 3 m. Comparing with the function from aseismic design code of reinforced concrete buildings in Taiwan [41], it can be known that, in practice, the fundamental periods of the measured buildings are much shorter than the design values. Besides, using the small-level earthquake data at other high-rise RC buildings located in Hualien and other Cities, such as Taipei, Taichung, and Tainan, almost all of the natural periods of existing buildings are smaller than the design level [42]. However, the natural periods of buildings in Hualien City are much smaller. Because the natural periods of buildings depend on the stiffness of stories, the shorter natural periods indicate that the actual stiffnesses of buildings in Hualien City are higher than buildings in other places. One of the possible reasons is the high stiffness of the nonstructural walls of buildings in Hualien City considered the high seismicity of this area during the construction.

From the results of questionnaire survey in the previous section, damages at the buildings of Group C are the most serious. However, there is no relationship can be seen between the characteristics of synthetic strong ground motions and the building damages for the buildings of this group. One of the reasons is the absence of velocity profile of ground structures at the sites of these buildings. The data at the sites of

HWA012 were used to calculate the strong ground motions. However, the ground structures at the sites of HWA012 and the site of buildings of Group C are different. The buildings of Group C are located at the boundary of two different geological conditions, which would amplify the ground motions due to constructive interference of seismic waves from different paths [43]. As if the irregular underground structure is validated, the amplification of ground motions at the sites of buildings of Group C can be examined with higher accuracy.

5. Conclusions

In this study, questionnaire surveys on feeling of shaking, indoor damages, structural and nonstructural damages at high-rise RC residential buildings due to the strong ground motions in the 2018 Hualien earthquake were performed. In this paper, answers to questionnaire survey were analyzed and compared by three building groups in terms of positions to the Milun fault and site conditions. It is found that damages at the buildings located on the central part of the hanging wall with relatively good site condition were the lightest for almost all the surveyed items. While, damages at the buildings located on the southwest and the northeast to the Milun fault were serious. Furthermore, the cracks in interior walls and concrete members at the buildings located on the northeast to the Milun fault were the most serious. It is speculated that long-duration shaking at the buildings of this group is one of the reasons of serious building damages.

A characterized seismic source model of the 2018 Hualien earthquake was proposed based on the Lee's [6] source model inversion results. The synthetic waveforms and response spectra at the strong ground motion stations are in good agreement with those of observed strong ground motions. In this model, the Milun fault was triggered by the west-dipping fault as a passive even. Horizontal ground motions were mainly generated by the rupture of Milun fault. Moreover, the south part of the Milun fault contained two main ground motion generation areas. One is a shallower SMGA (SMGA7) with long rise-time of 2.6 s, the other is a deeper SMGA (SMGA8) with short rise-time of 1.2 s. The SMGA7 and SMGA8 contribute to the horizontal ground motions in the NS direction and the EW direction, respectively.

Strong ground motions at the sites of buildings for questionnaire survey were synthesized using thin layer method. Pulse-like ground motions are pronounced at all the sites of buildings. Due to the rupture directivity effect of the south part of Milun fault, the values of PGVs and the maximum values of the pSv are the highest at the sites of buildings located on the southwest of the Milun fault. The high amplitude of strong ground motions on the south part of the Milun fault, which were generated by the directivity effect, is one of the reasons for serious building damages [44–46]. The peaks of the pSv spectra in the period range of 2 s–3 s are generated by SMGA7. There are two reasons for the peaks in the period range of 1 s–2 s. One is the site amplification, the other is the source effect from the SMGA8. The fundamental periods of the buildings for questionnaire survey are in the range of 0.3 s–0.7 s. The predominant periods at the ground in the Hualien City are almost in the range of 0.5 s–1 s. Because the non-linear response will enlarge the periods of buildings, the pulses with period in the range of 1 s–2 s are considered to be dangerous to high-rise buildings and caused building damages.

Because the data of ground structures at the sites of buildings in the northeast group (Group C) was unavailable, it is difficult to rigorously discuss the relationship between building damage and characteristics of strong ground motions in this region. Furthermore, the buildings of Group C are located at the foot of a hill. There is a possibility of large amplification due to the tomography during the earthquake. The plane shapes of the surveyed buildings in Group C are complicated as in the shape of letter "H". There is a possibility that complex vibration modes such as torsional vibration and local deformation of floors may occur during the earthquake. In future work, it is necessary to construct a three-dimensional model of the buildings in Group C to perform more

rigorously study on the correspondence of responses to synthesized ground motions with the damages to the buildings.

Declaration of competing interest

The authors declare that they have no known competing financial interests or personal relationships that could have appeared to influence the work reported in this paper.

References

[1] T. Hida, M. Nagano, Indoor damages of super high-rise residential buildings during the 2011 off the pacific coast of Tohoku earthquake based on strong motion records and questionnaire survey, J. Struct. Constr. Eng., AIJ 77 (677) (2012) 1065–1072.

[2] M. Nagano, S. Watanabe, Y. Hinoura, K. Suzuki, Shaking and indoor damages of super high-rise residential buildings during the 2016 Kumamoto earthquake based on questionnaire survey, AIJ J. Technol. Des. 24 (57) (2018) 565–570.

[3] H. Kanamori, L. Ye, B.S. Huang, H.H. Huang, S.J. Lee, W.T. Liang, Y.Y. Lin, K.F. Ma, Y.M. Wu, T.Y. Yeh, A strong-motion hot spot of the 2016 Meinong, Taiwan, earthquake (Mw 6.4), Terr. Atmos. Ocean Sci. 28 (2017) 637–650, https://doi.org/10.3319/TAO.2016.10.07.01.

[4] K.F. Ma, Y.M. Wu, Preface to the focus section on the 6 february 2018Mw 6.4 hualien, taiwan, earthquake, Seismol. Res. Lett. December 12 90 (2018) (2019) 15–18, https://doi.org/10.1785/0220180356.

[5] Y.H. Yang, J.C. Hu, H. Tung, M.C. Tsai, Q. Chen, Q. Xu, Y.J. Zhang, J.J. Zhao, G. X. Liu, J.N. Xiong, J.Y. Wang, B. Yu, C.Y. Chiu, Z. Su, Co-seismic and postseismic fault models of the 2018 Mw 6.4 hualien earthquake occurred in the junction of collision and subduction boundaries offshore eastern taiwan, Rem. Sens. 2018 (10) (2018) 1372, https://doi.org/10.3390/rs10091372.

[6] S.J. Lee, T.C. Lin, T.Y. Liu, T.P. Wong, Fault-to-fault jumping rupture of the 2018 MW 6.4 hualien earthquake in eastern taiwan, Seismol Res. Lett. 90 (No.1) (2019) 30–39.

[7] Y.Y. Wen, S. Wen, Y.H. Lee, K.E. Ching, The kinematic source analysis for 2018 Mw 6.4 Hualien, Taiwan earthquake, Terr. Atmos. Ocean Sci. 30 (2019) 1–10, https://doi.org/10.3319/TAO.2018.11.15.03.

[8] H. Kuo-Chen, Z.K. Guan, W.F. Sun, P.Y. Jhong, D. Brown, Aftershock sequence of the 2018 Mw 6.4 Hualien earthquake in eastern Taiwan from a dense seismic array data set, Seismol. Res. Lett. 90 (No.1) (2019) 60–67, https://doi.org/10.1785/0220180233.

[9] P.R. Jian, S.H. Hung, L.S. Meng, Rupture behavior and interaction of the 2018 Hualien earthquake sequence and its tectonic implication, Seismol. Res. Lett. 90 (No.1) (2019) 68–77, https://doi.org/10.1785/0220180241.

[10] T.L. Hsu, Earthquakes in taiwan, Q. J. Bank Taiwan 7 (2) (1955) 148–164 (in Chinese).

[11] C.C. Lin, The Quaternary of the Hualien Area - the Quaternary of Taiwan, National Council on Science Development Research Report, 1962, p. 42 (in Chinese).

[12] S.B. Yu, D.D. Jackson, G.K. Yu, C.C. Liu, Dislocation model for crustal deformation in the Longitudinal Valley area, eastern Taiwan, Tectonophysics 183 (1990) 97–109, https://doi.org/10.1016/0040-1951(90)90190-J.

[13] J.B.H. Shyu, Y.R. Chuang, Y.L. Chen, Y.R. Lee, C.T. Cheng, A new on-land seismogenic structure source database from the Taiwan Earthquake Model (TEM) project for seismic hazard analysis of Taiwan, Terr. Atmos. Ocean Sci. 27 (2016) 311–323, https://doi.org/10.3319/TAO.2015.11.27.02(TEM).

[14] S.Y. Huang, J.Y. Yen, B.L. Wu, I.C. Yen, R.Y. Chuang, Investigating the Milun fault: the coseismic surface rupture zone of the 2018/02/06 ML 6.2 Hualien earthquake, Taiwan, Terr. Atmos. Ocean Sci. 30 (2019) 1–25, https://doi.org/10.3319/TAO.2018.12.09.03.

[15] C.H. Kuo, J.Y. Huang, C.M. Lin, T.Y. Hsu, S.H. Chao, K.L. Wen, Strong ground motion and Pulse-like velocity observations in the near-fault region of the 2018 MW 6.4 Hualien, Taiwan Earthquake, Seismol. Res. Lett. 90 (No.1) (2019) 40–50.

[16] K.C. Lin, J.C. Hu, K.E. Ching, J. Angelier, R.J. Rau, S.B. Yu, C.H. Tsai, T.C. Shin, M. H. Huang, GPS crustal deformation, strain rate and seismic activity after the 1999 Chi-Chi earthquake in Taiwan, J. Geophys. Res.2010 115 (2010) B07404.

[17] R.-D. Hwang, C.-Y. Lin, C.-Y. Lin, W.-Y. Chang, T.-W. Lin, Y.-L. Huang, J.-P. Chang, Multiple-event analysis of the 2018 ML 6.2 Hualien earthquake using source time

functions, Terr. Atmos. Ocean Sci. 30 (2019) 1–10, https://doi.org/10.3319/TAO.2018.11.15.01.

[18] S.J. Chin, J.Y. Lin, Y.F. Chen, W.N. Wu, C.W. Liang, Transition of the Taiwan-Ryukyu collision-subduction process as revealed by ocean-bottom seismometer observations, J. Asian Earth Sci. 128 (2016) 149–157.

[19] F.T. Wu, W.-T. Liang, J.-C. Lee, H. Benz, A. Villasenor, A model for the termination of the Ryukyu subduction zone against Taiwan: a junction of collision, subduction/separation, and subduction boundaries, J. Geophys. Res. 114 (2009) B07404, https://doi.org/10.1029/2008JB005950.

[20] H. Kuo-chen, Y.M. Wu, C.H. Chang, J.C. Hu, W.S. Chen, Relocation of the eastern Taiwan earthquakes and its tectonic implications, Terr. Atmos. Ocean Sci. 15 (2004) 647–666, https://doi.org/10.3319/TAO.2004.15.4.647(T).

[21] Y.C. Yang, Earthquakes in Hualien in the latest 41 years, Hualien Literat. 1 (1953) 67–71 (in Chinese).

[22] T.L. Hsu, Recent faulting in the Longitudinal Valley of eastern taiwan, Mem. Geol. Soc. China 1 (1962) 95–102.

[23] C.Y. Chen, J.C. Lee, Y.G. Chen, R.F. Chen, Campaigned GPS on present-day crustal deformation in northernmost Longitudinal Valley preliminary results, hualien taiwan, Terr. Atmos. Ocean Sci. 25 (2014) 337–357, https://doi.org/10.3319/TAO.2013.12.25.01.

[24] Y.-C. Hsu, C.-P. Chang, J.-Y. Yen, H. Kuo-Chen, C.-C. Wang, Investigating the structure of the Milun fault from surface ruptures of the 2018 hualien earthquake, Terr. Atmos. Ocean Sci. 30 (2019) 1–14, https://doi.org/10.3319/TAO.2018.09.28.01.

[25] Y.S. Lin, R.Y. Chuang, J.Y. Yen, Y.C. Chen, Y.T. Kuo, B.L. Wu, S.Y. Huang, C.J. Yang, Mapping surface breakages of the 2018 Hualien earthquake by using UAS photogrammetry, Terr. Atmos. Ocean Sci. 30 (2019) 1–16, https://doi.org/10.3319/TAO.2018.12.09.02.

[26] J.Y. Yen, C.H. Lu, R.J. Dorsey, K. Ch Hao, C.P. Chang, C.C. Wang, R.Y. Chuang, Y.T. Kuo, C.Y. Chiu, Y.H. Chang, F. Bovenga, W.Y. Chang, Insights into seismogenic deformation during the 2018 hualien, taiwan, earthquake sequence from InSAR, GPS, and modeling, Seismol Res. Lett. 90 (2019) 78–87, https://doi.org/10.1785/0220180228.

[27] Shengze Tian, G. Paolo, W. Ch Yuan, "Coseismic deformation of the 6 february 2018Mw 6.2 hualien earthquake based on strong-motion recordings", Seismol. Res. Lett. Nov. 28 90 (2018) (2019) 108–117, https://doi.org/10.1785/0220180235.

[28] J.Y. Yen, C.H. Lu, C.P. Chang, A.J. Hooper, Y.H. Chang, W.T. Liang, T.Y. Chang, M.S. Lin, K.S. Chen, Investigating active deformation in the northern Longitudinal Valley and City of Hualien in eastern Taiwan using persistent scatter and small-baseline SAR interferometry, Terr. Atmos. Ocean Sci. 22 (2011) 291–304, https://doi.org/10.3319/TAO.2010.10.25.01(TT).

[29] Y.L. Chen, T.C. Shin, Study on the earthquake location of 3-D velocity structure in the Taiwan area, Meteorol. Bull. 42 (2) (1998) 135–169 (in Chinese).

[30] C.M. Lin, C.H. Kuo, J.Y. Huang, H.H. Hsieh, C.C. Si, K.L. Wen, Shallow Shear-Wave Velocity Structures of TSMIP Stations in Taiwan, Technical Report of National Center for Research on Earthquake Engineering, NCREE-18-019, 2018, p. 141 (in Chinese).

[31] Central Geological Survey (CGS), Geology Survey Report of the 2018.02.06 Hualien Earthquake, Central Geology Survey, Ministry of Economic Affairs, Taipei, Taiwan, 2018 (in Chinese).

[32] C. Kitsunezaki, N. Goto, Y. Kobayashi, T. Ikawa, M. Horike, T. Saito, T. Kurota, K. Yamane, K. Okuzumi, Estimation of P- and S- Wave velocities in deep soil deposits for evaluating ground vibrations in earthquake, Japn. Soc. Natl. Disaster Sci. 9 (No. 3) (1990) 1–17.

[33] G.H.F. Gardner, L.W. Gardner, A.R. Gregory, Formation velocity and density - the diagnostic basics for stratigraphic traps, Geophysics 39 (Number 6) (1974) 770–780.

[34] M. Nagano, T. Watanabe, Improvement of calculation precision of theoretical ground motions using thin layer method and its verification, AIJ J. Technol. Design 13 (26) (2008) 451–456.

[35] Y. Hisada, M. Nagano, A. Nozu, K. Miyakoshi, K. Asano, T. Matsumoto, T. Nakagawa, Benchmark, Tests for strong ground motion prediction methods using theoretical methods, in: Proc. Of 15th World Conference on Earthquake Engineering, Lisbon, Portugal, 2012.9.24-30, Lisbon Congress Center, 2012.

[36] H. Tajimi, Contribution to theoretical prediction of dynamic stiffness of surface foundations, Proc. of 7th World Conf. Earthquake Eng. 5 (1980) 105–112.

[37] E. Kausel, An Explicit Solution for the Green's Functions for Dynamic Loads in Layered Media", Technical Report R81-13, Department of Civil Engineering, MIT, 1981.

[38] E. Kausel, Accurate stresses in the thin-layer element, Int. J. Numer. Methods Eng. 61 (2004) 360–379.

[39] J. Park, E. Kausel, Numerical dispersion in the thin-layer method, Comput. Struct. 82 (2004) 607–625.

[40] T. Watanabe, X. Wang, H.J. Si, W.Y. Chang, M. Nagano, Lessons learned from the 2018 Hualien earthquake: II. Nonlinear response analysis of high-rise buildings to pulse-like ground motions, in: International Conference in Commemoration of 20th Anniversary of the 1999 Chi-Chi Earthquake Taipei, Taiwan, September 15-19, 2019, 2019.

[41] Cpami, "Seismic Design Provisions and Commentary for Buildings", Construction and Planning Agency, Ministry of the Interior, Taiwan, R.O.C, 2011 (in Chinese).

[42] Z. Zhang, C.H. Kuo, X. Wang, M. Nagano, Dynamic characteristics of high-rise RC buildings in Taiwan using strong motion records, in: Annual Meeting of Architectural Institute of Japan, 2020, pp. 1039–1040.

[43] M. Motosaka, M. Nagano, Analysis of ground-motion amplification characteristics in Kobe City considering a deep irregular underground structure -interpretation of heavily damaged belt zone during the 1995 Hyoko-ken Nanbu Earthquake-, J. Phys. Earth 44 (1996) 577–590.

[44] Y.F. Vargas-Alzate, L.G. Pujades, A.H. Barbat, J.E. Hurtado, S.A. Diaz, D.A. Hidalgo-Leiva, Probabilistic seismic damage assessment of reinforced concrete buildings considering directionality effects, Struct. Infrastruct. Eng. 14 (6) (2018) 817–829.

[45] L.A. Pinzón, S.A. Díaz-Alvarado, L.G. Pujades, R.E. Alva, Do directionality effects influence the expected damage? A case study of the 2017 Central Mexico earthquake, Bull. Seismol. Soc. Am. 108 (5a) (2018) 2543–2555, https://doi.org/10.1785/0120180049. October 2018.

[46] L.A. Pinzón, S.A. Diaz, L.G. Pujades, Y.F. Vargas-Alzate, An efficient method for considering the directionality effect of earthquakes on structures, J. Earthq. Eng. (2019) 1–30, https://doi.org/10.1080/13632469.2019.1597783.